Summer 7-30-2024

The Role of Sensing Modalities in Shaping Collective Motion and Group Behavior

Poorendra P. Ramlall
Embry-Riddle Aeronautical University, ramlallp@my.erau.edu

The Role of Sensing Modalities in Shaping Collective Motion and Group Behavior

by

Poorendra Paul Ramlall

Submitted to the Department of Mechanical Engineering
in partial fulfillment of the requirements for the degree of

Master of Science in Mechanical Engineering

at the

EMBRY-RIDDLE AERONAUTICAL UNIVERSITY

July 2024

Author .....
Poorendra Paul Ramlall
Department of Mechanical Engineering
July 25, 2024

Certified by .....
Dr. Subhradeep Roy
Assistant Professor
Thesis Supervisor

Accepted by .....
Dr. Jean-Michel Dhainaut
Program Coordinator, MS Mechanical Engineering

The Role of Sensing Modalities in Shaping Collective Motion and Group Behavior

by

Poorendra Paul Ramlall

Submitted to the Department of Mechanical Engineering
on July 25, 2024, in partial fulfillment of the
requirements for the degree of
Master of Science in Mechanical Engineering

Abstract

Collective behavior refers to the coordinated movements that emerge from simple interactions between individuals within a group. Traditionally, researchers have modeled these interactions assuming individuals can sense their surroundings in all directions, like having eyes all around their heads. While this is a useful simplification, it does not capture the diverse ways animals actually sense the world. In this thesis, we take inspiration from the natural world, particularly from animals like bats and dolphins that use a combination of hearing and sight to navigate their environments. We explore how combining these sensory cues in a three-dimensional space affects the way groups move and behave. Our findings reveal that integrating auditory and visual information allows for more effective group coordination, combining the strengths of both senses. We also look at another fascinating aspect of animal behavior: some species pay attention to areas outside their direct line of movement. Imagine being able to know what is happening behind you while walking forward. We investigate how this kind of 'offset' sensing influences group dynamics. For instance, when the sensing field is directed opposite to the movement direction, unique and unexpected group behaviors emerge. Understanding these mechanisms can provide deep insights into the behavior of animal groups and inspire innovative designs for artificial systems, leading to better-coordinated and more efficient robotic swarms.

Thesis Supervisor: Dr. Subhradeep Roy
Title: Assistant Professor

Acknowledgments

The culmination of this work is bitter-sweet, filled with both contentment and a realization that all exiting work must come to an end, hopefully temporarily. Nevertheless, acknowledgements are in order to those without whom this work would not have been possible.

First and foremost, I would like to express sincere gratitude my advisor Dr. Subhradeep Roy for his continued patience, expertise, and support. Not only for these duties, but also for the invaluable guidance in both work and life. The countless hours of discussion on various topics truly help me develop to be a better person, and I would not be pursuing graduate studies (and higher) if not for your persistent encouragement.

Secondly, I would like to thank Dr. Magdy Attia, who inspired me to be a better engineer, and was instrumental in the success of my undergraduate education and my pursuit of graduate education. Additionally, I would like to thank Dr. Eric Coyle and Dr. Jean-Michel Dhainaut for their invaluable advice during my studies, as well as Dr. Sirish Namilae and Dr. Bryan Watson for serving on my thesis committee. Lastly, special thanks to Ms. Christina Groenenboom who seems to always have a solution to every logistical problem.

I must acknowledge my family, both near and far, for continued support. Special thanks to my parents for frequent visits, conversations, and love; and to my second family (the Bholas) who have made these past few years filled with love and care. I would be remiss to not express gratitude to my peers for the countless hours we spent working together, motivating each other, and making memories. Special mention is given to two of my best fiends, Plamen Petkov for working alongside me especially nearing the culmination, and Roman Morozov for his continued support and late night billiards matches. Thank you to all who have been beside me all this time - too many to mention. I would not be who I am and where I am today without the people in my life and the experiences that guided me.

Above all else, **Thanks be to God.**

This research was partially supported by the National Science Foundation under grant CMMI-2238359 and by the start-up fund from the College of Engineering at Embry-Riddle Aeronautical University - Daytona Beach

This graduate thesis has been examined by a Committee of the College of Engineering as follows:

Dr. Subhradeep Roy .....
Chairman, Thesis Committee; Thesis Supervisor
Assistant Professor of Mechanical Engineering

Dr. Bryan Watson .....
Member, Thesis Committee
Assistant Professor of Systems Engineering

Dr. Sirish Namilae .....
Member, Thesis Committee
Professor of Aerospace Engineering

Contents

List of Figures

Listings

Chapter 1

Collective behavior and collective behavior models

1.1 Introduction to collective behavior

Collective behavior refers to the coordinated actions and emergent patterns that arise from local interactions among individuals within a group, leading to complex and often emergent phenomena in both natural and artificial systems [1, 2, 3]. This *collective behavior* exist in the world in macro and micro scales [4], and may contain living and non-living entities [5, 6]. On a macro scale, systems that exhibit collective behavior include flocking birds [1] and schooling fish [7]. On a micro scale, examples of systems that exhibit collective behavior may be the movement, growth, and tracking of bacteria and white blood cells [8, 9, 10].

There are several biological advantages to collective motion in animal groups, usually relevant for survival. These include predation [11], foraging for food [12, 13], sharing information [14, 15], reproduction [16], or migration and defense [17]. In addition, group efficiency can be tailored through collective behavior where organisms can collectively execute the same tasks, or share the burden of group survival through highly specialized roles [18, 12]. This is especially prevalent in the case of foraging in insect colonies [19, 18], migration in bird flocks and fish schools [17, 12], coordinated hunting strategies of social predators such as dolphins, orcas, wolves, and peregrine

falcons [11, 16, 20], and movement strategies like those observed in elephant herds and muskoxen [21, 22].

Collective motion phenomena are not restricted to living matter, and in recent years have been studied in various experimental systems, such as active colloids, driven granular matter, and ferro-magnetic particles in the presence of a magnetic field [23, 24, 1, 2]. Though the emergent behavior is observable, the types of behaviors and many of the controlling factors still remain obscure for such systems.

1.2 Collective behavior models

The study of collective motion is an ongoing endeavor which has produced a variety of models attempting to replicate and describe the emergent behavior seen in nature. These models facilitate the investigation of these different systems in a simulation framework, and are used to provide some level of insight into how the dynamics of these systems change when subject to changes in both intrinsic and extrinsic parameters. The numerous models generally fall into three categories: phenomenological models, Eulerian models, and Lagrangian models [6].

Phenomenological models aim to explain collective behavior using simple mathematical formulations providing quantitative outcomes from a small number of tunable control parameters, generally analogous to systems with catalytic behavior [6]. A epitomic example is the use of non-linear differential equations to model the large-scale recruitment of ants for a task through chemotaxis with positive reinforcement from deposited pheromones [25, 26, 27]. Phenomenological models provide a general understanding of collective behaviour due to abstract reasoning and measurable parameters, but are often not rigid enough to provide mechanistic insight [28]. Phenomenological models, simplified from more complex models with numerous parameters, offer advantages by reducing the need for excessive control variables [29]. However, representing social interactions and sensory cues in these models remains challenging [30]. For example, in a phenomenological model of collective behaviour, the general behaviour of a swarm can be specified by a formula, however, if the method of information

gathering is changed, then the model loses its applicability as the assumption that the overall behaviour can be represented as an average is lost. Additionally, when different considering sensory cues, it may be difficult or impossible to obtain closed form expressions to represent these social interactions.

Eulerian models are useful for investigating patterns and large-scale behaviors. In this paradigm, the group is treated as a continuum and does not consider microscopic interactions, but relies on conservation laws for the development of group-level behavior [6, 1]. For example, Mogilner and Keshet model swarming behavior based on non-local interactions using an advection-diffusion basis [31]. One of the earliest of these investigations was a study conducted by Keller and Segel in 1971, motivated by the study of collective motion in bacteria colonies [32]. This study uses non-linear parabolic differential equations to model the movement of the *Escherichia coli* bacteria in the presence of a chemical stimulus. Comparing to the previously discussed chemotaxis study using the phenomenological model, we see that similar motivations can be investigated using different models subject to the desired level of granularity.

Lagrangian models, on the other hand, consider finer interactions and achieve collective behavior by describing the interactions between entities. The working principle is that the group-level behavior can be attributed to the local interactions between the individuals of the group - an idea mirrored in statistical mechanics [6, 2, 1]. For this reason, Lagrangian models are also called agent-based models [33, 34]. Unlike Eulerian models, agent-based models operate in discrete time, where the trajectories of the agents are computed at every time time step. The development of agent-based models have generally been motivated by biological swarming systems, such as bird flocks, where the driving force of decision making is influenced by direct interactions with other members of the group [6]. Agent-based modelling is a popular tool for research into biologically motivated collective behavior, especially when considering swarming behavior.

Of the various developed agent-based models, one of the most popular models used to simulate collective behavior is the Reynolds Boids model [17], first developed for computer animations of birds in 1987. In Reynolds' Boids model, the agents use

differential equations to steer themselves and execute three manoeuvres: avoiding nearby flock-mates, steering towards nearby flock-mates, and steering towards the center of mass of local flock-mates [17, 1]. A similar, albeit less famous, study was previously conducted by Aoki [35] in 1981 which aimed to model the schooling mechanism in fish for three manoeuvres: approach, avoidance, and movement in parallel orientations. Both Reynolds' model and Aoki's model consider approach and avoidance, however, the specific biological inspirations remain in each model: Reynolds considered the clustering of birds, while Aoki considered the parallel movement of fishes in schools.

Less overtly specific biologically inspired models have been developed with the intention of describing animal groups in general and not replicate a particular organism's behavior. Models, such as Couzin's model [36], approach the question differently and introduce zones of attraction and repulsion where the decision to aggregate or separate depends on the spatial distribution of the agents within these zones. In all these models, a great deal of consideration is given to the mathematical rules that govern these behavior, however, studies have indicated that explicit steering and alignment rules may force behavior not generally observed in the initially inspired biological systems, and need not be modelled [1]. In an effort to remedy this increasing constraint, agent-based models with more minimality have seen substantial development.

Minimal agent-based models

Minimal agent-based models rely on very simple mathematical rules to govern only local interactions between agents, and give rise complex emergent behavior dependent on a few tunable parameters. One of the most studied minimal agent based model is the original Vicsek model [2]. Developed by Tamás Vicsek in 1995, the genesis of the Vicsek model lies in an attempt to simulate biologically inspired collective behavior using a simple agent-based paradigm with limited rules [2]. The Vicsek model tackles a similar problem as Reynolds' Boids model, albeit with simpler mechanics. While each *boid* in Reynolds' model was an autonomous agent only taking partial influence

from its surrounding *boids*, the agents in the Vicsek model are infinitesimal point-like agents, with no autonomy and whose behavior is fully controlled by the properties of its neighboring agents [17, 2]. Additionally, instead of following a kinematic (or other rules to generate acceleration) model to inform motion, the motion of the agents in the Vicsek model is governed by a simple rule to update their heading: the agents maintain constant speed, and at every time step, they assume the average direction of motion of the agents within their defined neighborhood [2].

One of the interesting characteristics of the Vicsek model is its ability to capture the phase transition from disordered to ordered motion. In the original Vicsek model order spontaneously emerges when particles align their trajectories with those in a nearby neighborhood. This transition from a disordered state to an ordered state occurs as the average particle density increases and magnitude of the random perturbations decreases [2, 1]. The seminal study by Vicsek in 1995 [2] characterized the phase transitions in terms how aligned the agents were, however, further work using variant models have investigated phase transitions using different metrics for different emergent structures [37, 3]. Much work has been done using proposed variants of the Vicsek model, ranging from investigation of phase transitions [2, 37], quantifying information transfer [38], implementing biologically inspired sensing modalities [3], investigation of hydrostatics [39] and hydrodynamics [39], inclusion of both repulsive and attractive interactions [40], application to robotic systems [41, 42], or simply as a mathematical model for developing computational advances [40].

1.3 Sensing mechanisms

By and large, the majority of studies using the Vicsek model restrict their domains to two dimensions and utilise a mechanism akin to that of vision; there is a field-of-view within which neighbors exist [43, 44, 45, 46]. The study conducted by Roy and collaborators [3] investigated three biologically inspired sensing modalities, namely: vision, audition, composite (a combination of the vision and audition). The visual sensing mode is analogous to flocking birds that employ vision for social cues, while the

auditory mode may be used to more accurately study bats who use echolocation for social and collective behavior [47, 48, 38, 49]. The use of a composite (combined audio-visual) sensing may allow for the modelling of systems that employ sensory fusion for localization, as in the case of collections of aerial and ground vehicles [50, 51, 52]. Additionally studies have also shown that the efficiency of decision making is affected by the ability to sense relevant neighbors [53, 54], and thus, may be negatively affected when the distribution of neighbors around an agent is not uniform. Due to this anisotropy, the nearest observable neighbors are likely to exist on the sides of the focal agent as opposed to in the direction of motion [6]. This phenomenon is supported by empirical evidence within the observations of small groups of fishes [6, 55]. It is then prudent to investigate different sensing mechanisms and their effect on the emergent behavior. Additionally, because the original Vicsek model and subsequent research uses a two-dimensional arena, it is important to investigate the effect of different sensing mechanisms in three-dimensions as well, especially when considering the relevance and applicability to real-world scenarios. Since these modifications do not affect the dynamics of the Vicsek model, but instead changes how the agents sense influential neighbors, the investigation of sensing modalities can be used to elucidate general principles about the emergence of group-level properties and how the application of these sensing mechanisms with possible restrictions can inform other models in the areas of biology, physics, and even logistics.

1.4 This work

Sensing modalities are key to defining communications which determine how the group level behavior will emerge. The application of sensing modalities to the Vicsek model is useful for exploration of biological and engineering questions. The objective in this study is to explore different sensing modalities and how they impact the emerging collective behavior. The investigations presented in this work comprises of two sections. Section 2 studies the emergent behavior in three dimensions of the Vicsek model modified to simulate three biological sensing modalities: vision,

audition, and a composite. Section 3 modifies the two-dimensional Vicsek model consider neighbors not in the direction of motion, but in a field-of-view that is offset from that directional heading.

The work presented mainly considers emergent behaviour in terms of the aggregation and alignment. Typically, the emergent behavior of the agents in the system

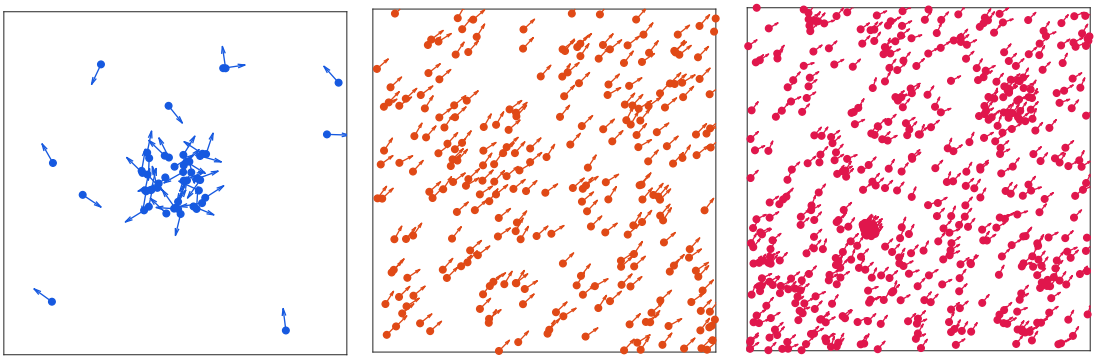

(a) (b) (c)

Figure 1-1: Different group-level behaviors: (a) A closely packed group with no group alignment; (b) A group collectively achieves a common heading direction, which emerges naturally based on interactions with neighbor; (c) A group with high group alignment and with some tightly packed clusters.

consist of three main qualities: aggregation, alignment, and some combination of the two. Figure 1-1a depicts the principle of aggregation, where the agents amass spatially with each other. Similarly, Figure 1-1b depict the principle of alignment, where the agents assume a coherent direction. Finally, Figure 1-1c shows an example where different group level formations may have a combination of properties. In this case, this formation has highly aligned and distributed agents, along with the formation of clusters.

Chapter 2

The role of sensory cues in collective dynamics: a study of three-dimensional Vicsek models

The content of this chapter is ready to be submitted for possible publication in a peer-reviewed journal.

2.1 Abstract

This study presents a three-dimensional collective motion model that integrates auditory and visual sensing modalities, inspired by species like bats that rely on these senses for navigation. Prior research predominantly focuses on vision-based sensing models, likely due to an inherent human bias towards vision. However, numerous species employ multiple sensory modalities. This study examines how combining these modalities influences group behavior in a generalized scenario of three-dimensional motion, an area not previously explored for combining sensory information. Using numerical simulations, we analyze the combined effects of auditory and visual sensing on group behavior, comparing them to the effects of using only vision or audition. The results demonstrate that composite sensing allows particles to interact with more neighbors, thereby gaining more information. This interaction enables the formation

of a single, large, perfectly aligned group within a narrow sensing region, a feature only achievable with vision at a wider field of view. Our findings demonstrate the importance of integrating multiple sensory modalities in shaping emergent group behavior, with potential applications in both biological studies and the development of robotic swarms.

2.2 Introduction

Collective behavior in animal groups involves the emergence of coordinated group-level patterns from local interactions among individuals. Each group member acts based on information received from local neighbors, leading to organized motion without any central leader. This behavior is prevalent in various biological systems, such as ant colonies [56], bird flocks [53], fish schools [57, 58], and mosquito swarms [59]. A significant advantage of group living is enhanced information access, aiding social animals in locating food [60], evading predators [61], and finding mates [62].

To understand the mechanisms behind group-level pattern formation from local interactions, various models have been proposed to simulate group coordination [63, 36, 64, 1, 65]. The mathematical modeling of collective behavior employs different approaches, such as continuous medium modeling [63], continuous-time modeling [64], and agent-based modeling in discrete-time [66]. A widely used agent-based model is the original Vicsek model [2], which operates on behavioral rules at the individual level. In the original Vicsek model, each individual moves at a constant speed within a two-dimensional space, aligning with the average direction of its neighbors while incorporating intrinsic noise to model individual randomness. Additionally, extrinsic noise, representing errors from environmental assumptions or information, can be considered [67]. The original Vicsek model defines neighbors as individuals within a circular sensing region around a given particle. Simulations reveal a phase transition from disordered to ordered states as the number of individuals or noise strength changes [2]. Studies indicate that intrinsic noise leads to a continuous phase transition, whereas extrinsic noise results in a discontinuous transition [67]. The simplicity of the

Vicsek model has inspired numerous variants, including models with both attractive and repulsive interactions [68, 69] and adaptations that extend the original model into more realistic three-dimensional scenarios [70]. Real-world biological swarms may not have omnidirectional vision, prompting modifications of the sensing region from a circular disk to a sector [45, 46, 71].

Most existing models of collective behavior assume visual cues for communication [44, 45, 46]. However, some social animals, such as bats and dolphins, rely on auditory cues [72]. There are few models that incorporate auditory interactions, such as those inspired by acoustic sensing in midges [73] and echolocation in bats [74]. A study in [3] explores auditory sensing in a modified two-dimensional Vicsek model, comparing it to visual sensing and demonstrating differences in group-level behavior. The auditory sensing is represented as a sector of a circle, mimicking the directivity pattern of ultrasonic beams observed in biological systems [75]. The results in [3] reveal that auditory sensing results in higher alignment and lower aggregation compared to visual sensing.

Despite advancements in studying group behavior through individual sensing cues, few models integrate multiple sensory modalities. However, empirical evidence, such as with bats, shows that they employ multimodal sensing—including audition, vision, somatosensory input, vestibular perception, and chemoreception—for navigation and communication [76, 75, 77]. Bats gather complementary information from vision and audition; vision helps detect long-range objects, while audition aids in accurately detecting small objects [77]. Multisensory integration offers several advantages, such as reduced reaction times [78]. Studies show that bats rely more on multimodal sensing in low-light conditions and adjust their behavior based on both visual and auditory inputs [79, 80, 81, 82, 83]. This empirical evidence supports the importance of multisensory integration in enhancing group behavior.

Improving our understanding of how multimodal sensing impacts group behavior is essential. Previous approaches, like the graph-theoretic method using consensus and synchronization protocols [84, 85], analyze the impact of multiple sensing modalities but overlook spatial distribution. The study in [86] introduces a composite

model that integrates auditory and visual cues however the model is restricted to two dimensions. Extending collective behavior models to three dimensions is crucial because it aligns more closely with the natural environments where these behaviors occur. Many animal groups, such as bird flocks, fish schools, and bat swarms operate in three-dimensional spaces, and their interactions can be significantly different from two-dimensional approximations [87, 88]. Three-dimensional models provide a better understanding of the dynamics and can capture phenomena that are not observable in two-dimensional models, such as complex evasive maneuvers and spatial formations [89, 90]. Therefore, incorporating three-dimensional extensions in collective behavior models is essential for accurately representing and analyzing real-world scenarios.

In this paper, we present three collective motion models: one with visual sensing, one with auditory sensing, and a composite model integrating both auditory and visual sensing, all explored in three dimensions for the first time. We conduct simulations to investigate how these sensory cues influences group behavior, measured by various order parameters.

2.3 Modeling

In this section, we outline the three-dimensional (3D) Vicsek framework and introduce our modifications to incorporate visual, auditory, and composite modalities through sensory neighbor interactions. Subsequently, we define the order parameters used to characterize collective behavior.

2.3.1 System dynamics

The 3D Vicsek model consists of N particles that move within a cubic domain of side length L, with the average particle density given by $\rho = N/L^3$. The model assumes that each agent travels at a constant speed, and the domain has periodic boundary conditions. In the original Vicsek model, every particle has a spherical sensing region with a radius R. Particles within this radius, including the particle

itself, are considered its 'neighbors'. During each discrete-time step, a particle updates its heading direction to align with the average direction of its neighbors.

The position of particle i at time step k, is given by the vector $\mathbf{x}_i(k) \in \mathbb{R}^3$, and its direction of motion is represented by the unit vector $\mathbf{v}_i(k) \in \mathbb{R}^3$. The heading direction of this particle i at the next time step $k+1$ is updated as follows:

$$\mathbf{v}_i(k+1) = \mathcal{N}\left(\mathcal{N}\left(\sum_{j\in\Lambda_i(k)} \mathbf{v}_j(k)\right) + \xi_i(k)\right), \tag{2.1}$$

where $\mathcal{N}(\mathbf{u}) = \mathbf{u}/\|\mathbf{u}\|$ represents the unit vector in the direction of $\mathbf{u}$, and $\Lambda_i(k)$ is the set of neighbors for particle i including itself that lie within a sphere of radius R centered at $\mathbf{x}_i(k)$. The vector $\xi_i(k)$ introduces intrinsic (process) noise to the heading direction, deviating it from the average neighbors' heading and is uniformly sampled from a sphere with a radius of η. Finally, the position update for particle i is given by:

$$\mathbf{x}_i(k+1) = \mathbf{x}_i(k) + v_0\mathbf{v}_i(k+1), \tag{2.2}$$

where v_0 represents the constant speed, assumed to be the same for all particles at all times.

2.3.2 Sensing modalities

We employ the same update protocol described above but modify the sensing regions to implement visual, auditory, and composite modalities. The primary difference between the visual and the auditory modalities lies in the index set of neighbors, $\Lambda_i(k)$. For visual sensing, each particle's field of vision is modeled as a spherical cone with radius R, symmetric about the its current heading direction. The cone represents *field of vision* with an opening angle of 2ϕ, where ϕ can range from 0 to π. When $\phi = \pi$, this model simplifies to the original 3D Vicsek model, where a particle's interaction neighborhood forms a sphere. At each time step, the visual neighbors comprises of the particles within an individual's field of vision.

For auditory sensing, an *acoustic beam* for each particle is modeled as a spherical

cone, mimicking the directivity pattern of ultrasonic beams observed in biological systems [75]. We assume the spherical cone is symmetric about the particle's current heading direction. Similar to the visual field, the acoustic beam has an opening angle of 2ϕ, with ϕ varying from 0 to π. A particle's auditory neighbors are those who it can 'hear' from. Thus, the auditory neighbors for a particle includes all the particles whose acoustic beams intersect with it.

To implement *composite sensing*, we independently construct the auditory and visual schemes and then combine these two modes to determine the neighbors of an individual at each time step. Consequently, the index set of neighbors for the ith particle at time step k in a composite sensing is given by

$$^{C}\Lambda_i(k) = {}^{V}\Lambda_i(k) \cup {}^{A}\Lambda_i(k),$$

where the left-superscripts C, V, and A represent composite, visual, and auditory modalities, respectively. This means that in composite sensing, the neighbors of an individual include particles who it can both 'see' and 'hear', without repetition. Figure 2-1 illustrates the schematic of the three interaction modes.

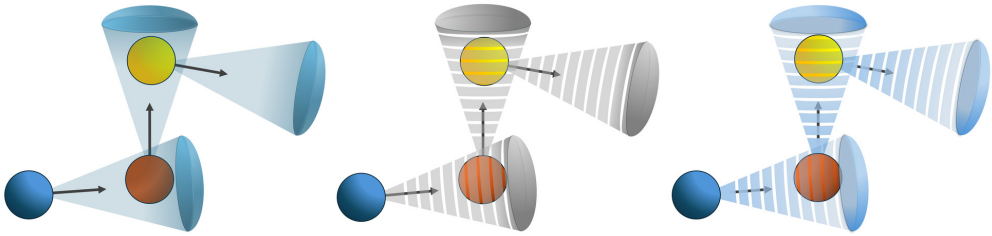

(a) (b) (c)

Figure 2-1: Schematic explaining the implementation of sensing modalities, where both the field of vision and the acoustic sonar are modeled as spherical cones in three dimensions. (a) In the visual mode, the orange has the yellow particle as its neighbor, but not the blue, since the yellow resides within its field of vision. (b) In the auditory mode, the orange has the blue particle as its neighbor, but not the yellow, since orange resides within the acoustic coverage of the blue and thus can hear it. (c) In the composite mode, the orange particle can 'see' the yellow and 'hear' the blue, making both yellow and blue its neighbors.

2.3.3 Order parameters

Next, we define the order parameters used to describe collective behavior.

The first order parameter is polarization, which quantifies group alignment. It is calculated as the average linear momentum of the system:

$$P(k) = \frac{1}{N} \left\| \sum_{i=1}^{N} \mathbf{v}_i(k) \right\|,$$

where $\|\cdot\|$ denotes the norm of the vector. Polarization values range from zero to one, with higher values indicating a more aligned group.

The second order parameter is cohesion, which measures how particles are spatially arranged in relation to the group's center of mass. At time step k, the group's center of mass is calculated as $\mathbf{X}(k) = (1/N) \sum_{i=1}^{N} \mathbf{x}_i(k)$, and the position of each particle relative to this center is given by $\mathbf{r}_i(k) = \mathbf{x}_i(k) - \mathbf{X}(k)$. Cohesion is then defined as:

$$C(k) = \frac{1}{N} \sum_{i=1}^{N} \exp\left[-\frac{\|\mathbf{r}_i(k)\|}{l_a} \right],$$

where we set the scaling coefficient $l_a = 4R$, following the study by [64]. Cohesion ranges from zero to one, where one indicates all particles reside at the center of mass, and zero indicates particles are infinitely far from the center of mass. Due to the periodic boundary conditions in a finite arena, the system cannot achieve a cohesion value of zero.

The third order parameter is cluster size, which represents the size of the largest weakly connected component in the interaction graph at a given time [3]. Two particles are part of the same cluster if they are connected by a path of interacting particles.

2.4 Results and discussion

We carry out numerical simulations to examine how combined visual and auditory cues affect group-level behavior, comparing these effects to those of purely visual and

auditory cues. In the composite model, each particle has two distinct sensing cones: one for the field of vision and the other for the acoustic beam. In this study, we ensure that the sensing cones for three different modalities are geometrically similar when comparing group behaviors across these modalities. This approach enables us to attribute any observed differences in group behavior to the nature of the sensing cues themselves rather than to variations in the size of the sensing regions. In other words, for any given simulation, the values of the sensing radius R and the sensing angle ϕ for auditory sensing are matched with those for visual sensing, and thus for the composite sensing, which combines auditory and visual sensing regions. Note that although the sensing cones for auditory and visual modalities are geometrically identical, the method of defining neighbors in each modality differs, leading to distinct sets of neighbors for each particle.

In our simulations, we set the side length of the cubic domain to $L = 5$, the constant particle speed to $v_0 = 0.03$, and the radius of the sensing cones for both auditory and visual modalities to $R = 1$. The initial positions and heading vectors of the particles are randomly selected within the cubic domain of side length L and the unit sphere, respectively, using uniform distributions. Sample simulation snapshots for the auditory, visual, and composite sensing modalities at time step $t = 100$, with parameters $\rho = 10$, $\eta = 0.2$ and $\phi = 2\pi/15$, are presented in Figure 2-2. We observe distinct group-level behavior emerge due to the differences in sensing modalities used.

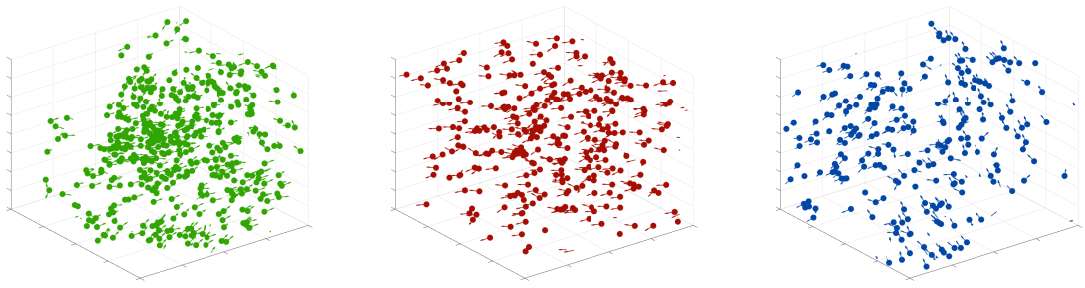

(a) (b) (c)

Figure 2-2: Partial domain visualization of 3D simulation of the Visual (2-2a) Auditory (2-2b) and Composite (2-2c) sensing modalities, for parameters $\rho = 5$, $\eta = 0.2$, and $\phi = \frac{2\pi}{15}$, at time step $t = 100$.

To further explore these differences, we examine the evolution of group alignment over time. Considering the presence of the generated uniform random noise in the system, we perform a Monte Carlo simulation for 1000 time-steps with 20 repetitions. Initial conditions are randomly generated from a uniform distribution and used across simulations. This ensures that the agents are initially in an unaligned state and distributed uniformly across the domain. While keeping the initial conditions fixed, we vary five specific pairs of parameters to reflect increasing noise levels and varying sensing angles as (η, ϕ) : $(0.1, 2\pi/15)$, $(0.3, 2\pi/15)$, $(0.5, 3\pi/15)$, $(0.7, 5\pi/15)$, and $(0.8, 4\pi/15)$. The results are presented in Figure 2-3. Each sub-figure plots the polarization as a function of time, with green lines representing visual, red lines representing auditory, and blue lines representing composite modalities. The dotted lines show the results from individual repetitions for each modality, while the dark continuous lines represent the averages computed over 20 repetitions at each time step.

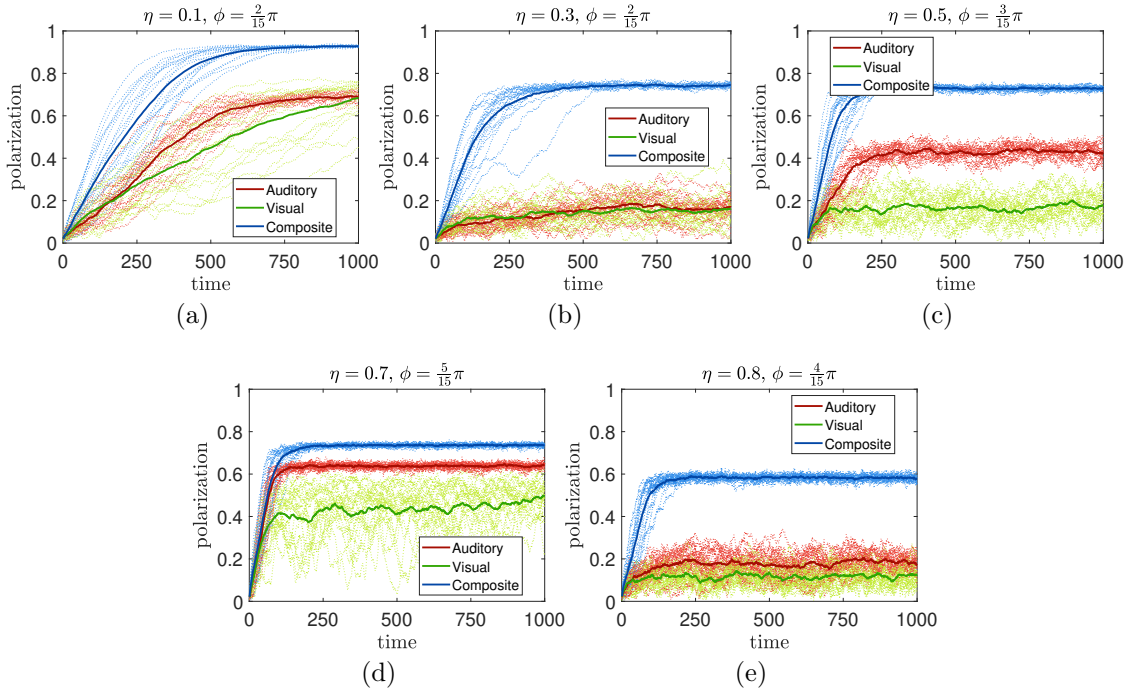

Figure 2-3: Monte Carlo simulations of polarization over 20 iterations for five different pairs of parameters comparing three modalities at $\rho = 2$.

For all five parameter sets, we observe that composite sensing results in a higher

degree of alignment, as indicated by high polarization values, when compared to both visual and auditory sensing modalities. Pure auditory sensing, on the other hand, when compared with pure visual sensing, results in faster or higher group alignment in certain instances. For example, as shown in Figure 2-3a with parameters $(\eta, \phi) = (0.1, 2\pi/15)$, both visual and auditory sensing achieve a polarization around 0.7, with auditory sensing reaching this value faster. Moreover, in Figures 2-3c, 2-3d, and 2-3e, auditory sensing consistently exhibits higher polarization compared to visual sensing. We also observe the dependence of group alignment on noise intensity and the sensing angle when comparing the sub-figures. For instance, comparing sub-figures 2-3a and 2-3b, where the sensing angle is fixed at $\phi = 2\pi/15$, an increase in noise intensity from $\eta = 0.1$ to $\eta = 0.3$ results in a decrease in polarization for each modality. Moreover, when the noise level is increased further from $\eta = 0.3$ to $\eta = 0.5$, an increase in the sensing angle from $\phi = 2\pi/15$ to $3\pi/15$, results in regaining group alignment, as observed in the comparison between sub-figures 2-3b and 2-3c. These results indicate an interplay between noise intensity and sensing angle that dictates the resultant group behavior. To further explore this relationship, we conduct a thorough investigation using a broader set of parameters, as well as examining additional characteristics of group behavior, including cohesion and cluster size.

Outside of the Monte-Carlo environment, we compare three distinct modalities, maintaining consistent initial positions and heading directions of the particles, which are randomly assigned as before. The simulations are run over the time interval $[0, 10000]$, with the initial transient period of 5000 time steps excluded from the analysis. To compare group-level behavior, we calculate three observables, which include the mean polarization, mean cohesion, and mean size of the largest cluster, averaged over the last 5000 time-steps.

The results are illustrated in Figure 2-4. The left, middle, and right columns correspond to the auditory, visual, and composite modes, respectively. The first, second, and third rows display the mean polarization, mean cohesion, and mean largest cluster size, respectively. In each plot, the two control parameters, noise

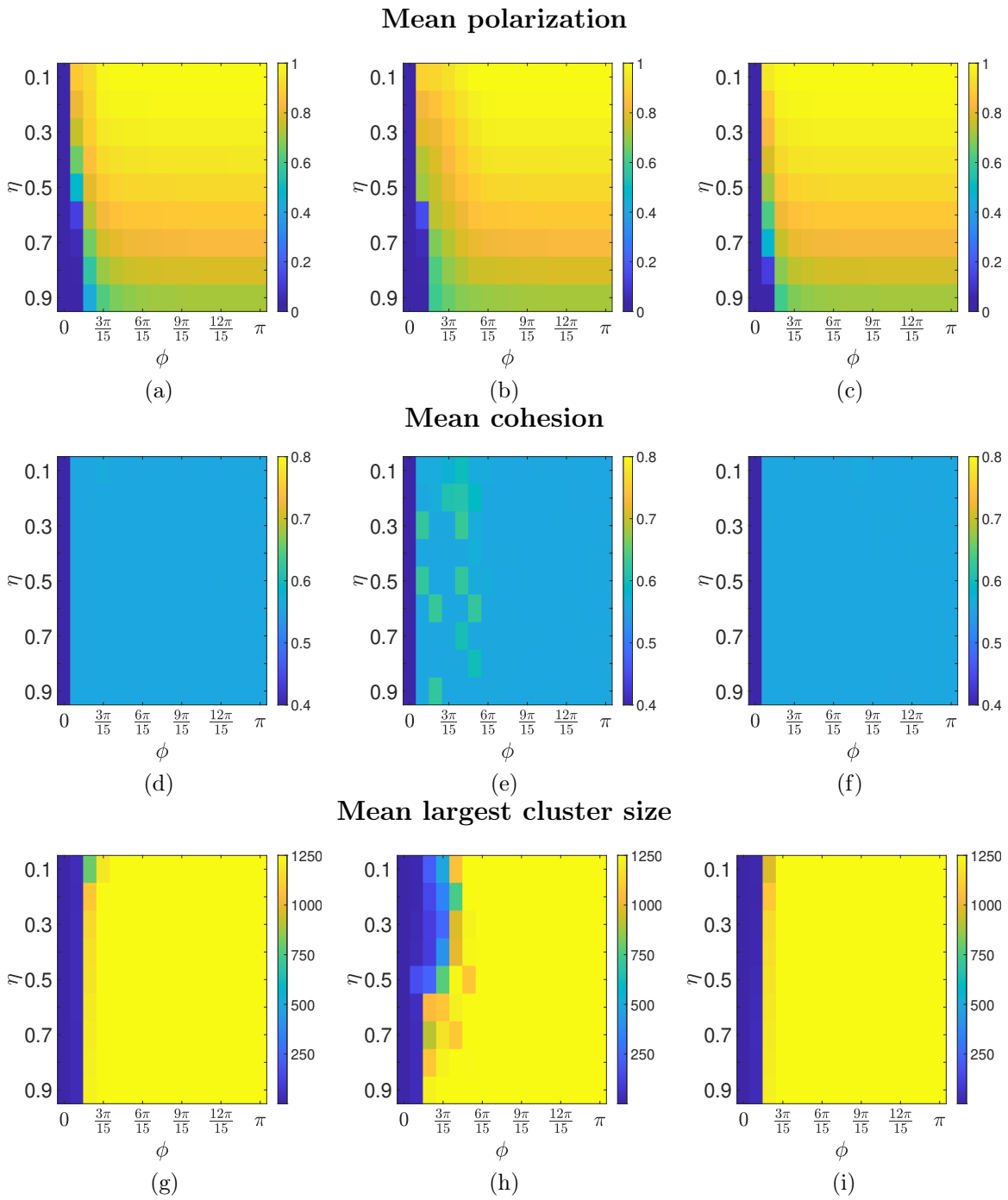

Figure 2-4: Results of the order parameter analysis comparing three modalities. Mean polarization (top row), mean cohesion (middle row), mean largest cluster size (bottom row) are calculated for auditory (left column), visual (middle column), and composite sensing (right column) modes.

intensity η and sensing angle ϕ, are varied. Specifically, η ranges from 0.1 to 0.9 in increments of 0.1, and ϕ ranges from 0 to π in increments of $\pi/15$.

By examining the three plots in Figures 2-4a - 2-4c, we observe that the mean polarization values are zero when $\phi = 0$, regardless of the noise intensity η. This occurs because $\phi = 0$ implies that particles lack any sensing capability, resulting in no interactions and thus a random walk behavior. Additionally, a sensing angle of $\phi = \pi$ establishes a spherical sensing neighborhood for the particles across all three sensing schemes, similar to the original Vicsek model. As expected, with a sensing angle of $\phi = \pi$, we observe that polarization decreases with increasing noise intensity, which is consistent with the findings from the original Vicsek model. This trend of decreasing polarization with increasing noise is also observed for other values of sensing angles for all three modalities.

Interestingly, for small noise intensities, we observe that polarization values are also sensitive to the sensing angle. For instance, in all three sensing modalities, when the sensing angle is reduced from a sphere to a cone, the polarization values decrease. This effect can be attributed to the smaller sensing regions, which result in fewer neighbors from which each particle can gather information, thereby impacting group alignment.

To compare the sensing modalities, we observe notable differences in polarization values when noise intensities are low and sensing angles are small. For example, when $\eta = 0.2$ and $\phi = 2\pi/15$, polarization in the composite modality reaches a perfect value of one, indicating complete group alignment. In contrast, at these parameter values, polarization in the auditory modality is slightly lower (around 0.9), which is still greater than the polarization observed in the visual modality (around 0.8). Alternatively, the visual mode requires a larger sensing angle of $\phi = 5\pi/15$ at this noise intensity to achieve perfect polarization, whereas the auditory mode can achieve this level of alignment with a smaller sensing region of $\phi = 3\pi/15$. In comparison, the composite mode attains perfect polarization with an even smaller sensing angle of $\phi = 2\pi/15$. From these observations, we conclude that the auditory mode allows particles to achieve perfect group alignment with a smaller sensing neighborhood

compared to the visual mode. In contrast, the composite mode enables perfect group alignment even when the sensing neighborhood is narrower. This is because, in the composite mode, particles benefit from the combined information from both auditory and visual sensing.

Next, we compare the group-level behavior in terms of mean cohesion (Figures 2-4d - 2-4f) and mean largest cluster size (Figures 2-4g - 2-4i) between the modalities. The largest cluster size is limited to the total number of agents, $N = 1250$, which occurs when the entire group forms a single large cluster. In the visual mode, when the sensing angle is small ($\pi/15 \leq \phi \leq 6\pi/15$), we observe higher cohesion values and smaller largest cluster sizes compared to the auditory mode. This behavior discrepancy between the two modalities can be explained by the formation of multiple clusters in the visual mode within this range of sensing angles. In these clusters, particles are densely packed, resulting in higher cohesion. However, because these clusters are disjoint, the largest cluster size is smaller. The formation of multiple clusters in the visual mode also leads to lower group alignment, as these individual clusters move in different directions. This reduces polarization values, as shown in Figure 2-4b. Conversely, in the auditory mode, within the same sensing angle range ($3\pi/15 \leq \phi \leq 6\pi/15$), the entire group typically forms a single large cluster (Figure 2-4g). However, the particles are more evenly distributed in space, resulting in relatively lower cohesion values compared to the visual mode.

In the composite sensing mode, as illustrated in Figures 2-4f and 2-4i, we observe that group cohesion is lower, and particles begin to form a single large cluster at a relatively smaller sensing angle of $\phi \geq 3\pi/15$ compared with visual mode. The findings suggest that the group behavior in the composite mode closely resembles that of the auditory mode, where particles coalesce into a single large cluster with common heading direction, resulting in a polarization value of one. However, the particles within the cluster are uniformly dispersed throughout the entire arena, resulting in reduced cohesion. In other words, in the composite sensing mode, auditory sensing plays a dominant role in determining group behavior.

2.4.1 Additional investigations

Comparison to 2D results

In the interest of completeness, additional investigations are conducted. First the results of the three sensing modalities shown in Figure 2-4 are compared to the findings in the study conducted by Roy and Lemus, who originally proposed and investigated these sensing modalities in [86]. The findings of this study correspond with those of the two-dimensional model in [86]. In both cases, agents using composite sensing interact with a larger set of neighbors, at lower sensing angles. This phenomena is even more prevalent in the three-dimensional implementation and lends credence to the idea that the added benefit of extending the model to three dimensions is non-trivial. Additionally, in both models, the composite sensing mode is dominated by audition, and audition itself has higher number of interacting agents at lower sensing angles compared to visual sensing.

The difference in polarization between the auditory sensing mode and the visual sensing mode is less distinct in the 3D model compared to the 2D model, however the agents still maintain higher alignment at lower sensing angles in the auditory mode. Increasing noise has a more negative effect on polarization for all three sensing modalities in the 3D model, resulting in lower polarization at high noise even at large sensing angles. In contrast, in the 2D model, the debilitating effects of increasing noise on polarization is redeemed by increasing sensing angles.

With regards to cohesion, both models maintain relatively low cohesion in all three sensing modalities, however the differences are less distinct in the 3D model. Nevertheless, both models show the formation of multiple clusters in the visual sensing mode, indicated by higher cohesion values paired with lower number interacting agents (cluster size).

In summary, the group level behaviour of the agents with different sensing modalities in the 3D model are consistent with the findings in the study conducted with the 2D model.

Sensitivity analysis of density

The study by Roy et.al in [3] considered the effect of density on the emergent behavior characterized by the order parameters for different sensing modalities in a two-dimensional model. Consequently, we also investigate the group-level order parameters at lower and higher densities of $\rho = 5$ and $\rho = 20$, simulated for 2000 time steps, the results of which are shown in Figure 2-5 and Figure 2-6, respectively.

In our initial analysis ($\rho = 10$) shown in Figure 2-4, there is a clear progression into phase transition from disordered to ordered motion as the sensing angle is increased, and differences between the sensing modalities can be ascertained. Decreasing the density from $\rho = 10$ to $\rho = 5$, as shown in Figure 2-5, results in less obvious distinctions between sensing modalities. The subtle differences in polarization and cohesion disappear, and the ability to identify emergent structures by considering the number of interacting agents is lost.

Conversely, increasing the density from $\rho = 10$ to $\rho = 20$, as shown in Figure 2-6, reveals more distinguishing features about the sensing modalities. In Figure 2-6c, the polarization in the composite sensing mode is revealed to be more sensitive to increasing noise. Considering the persistent low cohesion with high cluster sizes, this may indicate the breaking and forming of clusters, or the formation of bands characterized by spatially aggregated agents but with less aligned directions. This phenomena occurs as the noise increased past a threshold of $\eta = 0.7$.

The pattern of increasing sensing angles having less redeeming effects at high noise is present at higher and lower densities. Similarly, the polarization does increase faster in the auditory mode compared to the visual mode. The overall trends in the group level behavior is maintained with increasing density.

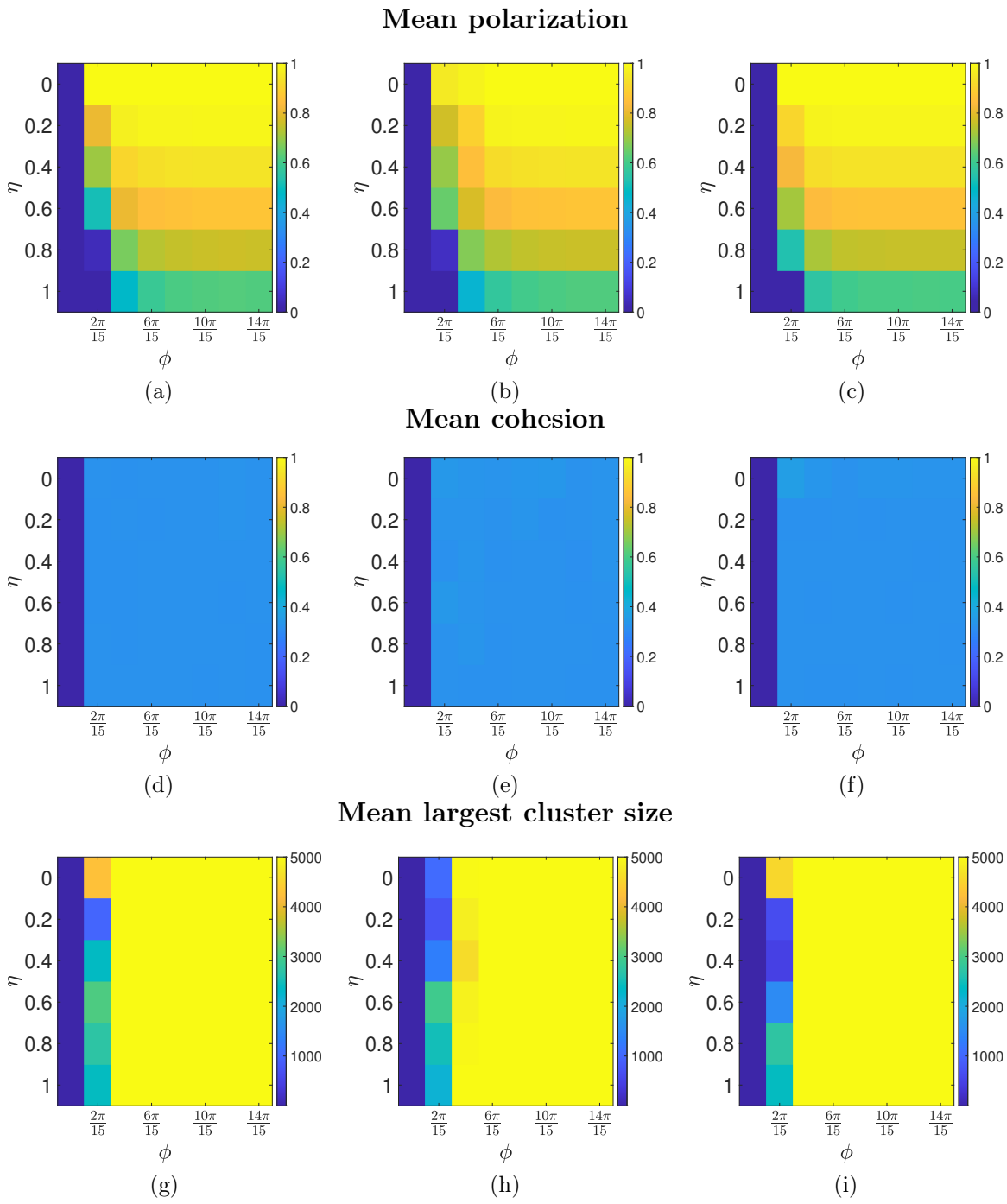

Figure 2-5: Order parameter results at $\rho = 5$ simulated for 2000 time steps. Mean polarization (top row), mean cohesion (middle row), mean largest cluster size (bottom row) are calculated for auditory (left column), visual (middle column), and composite sensing (right column) modes.

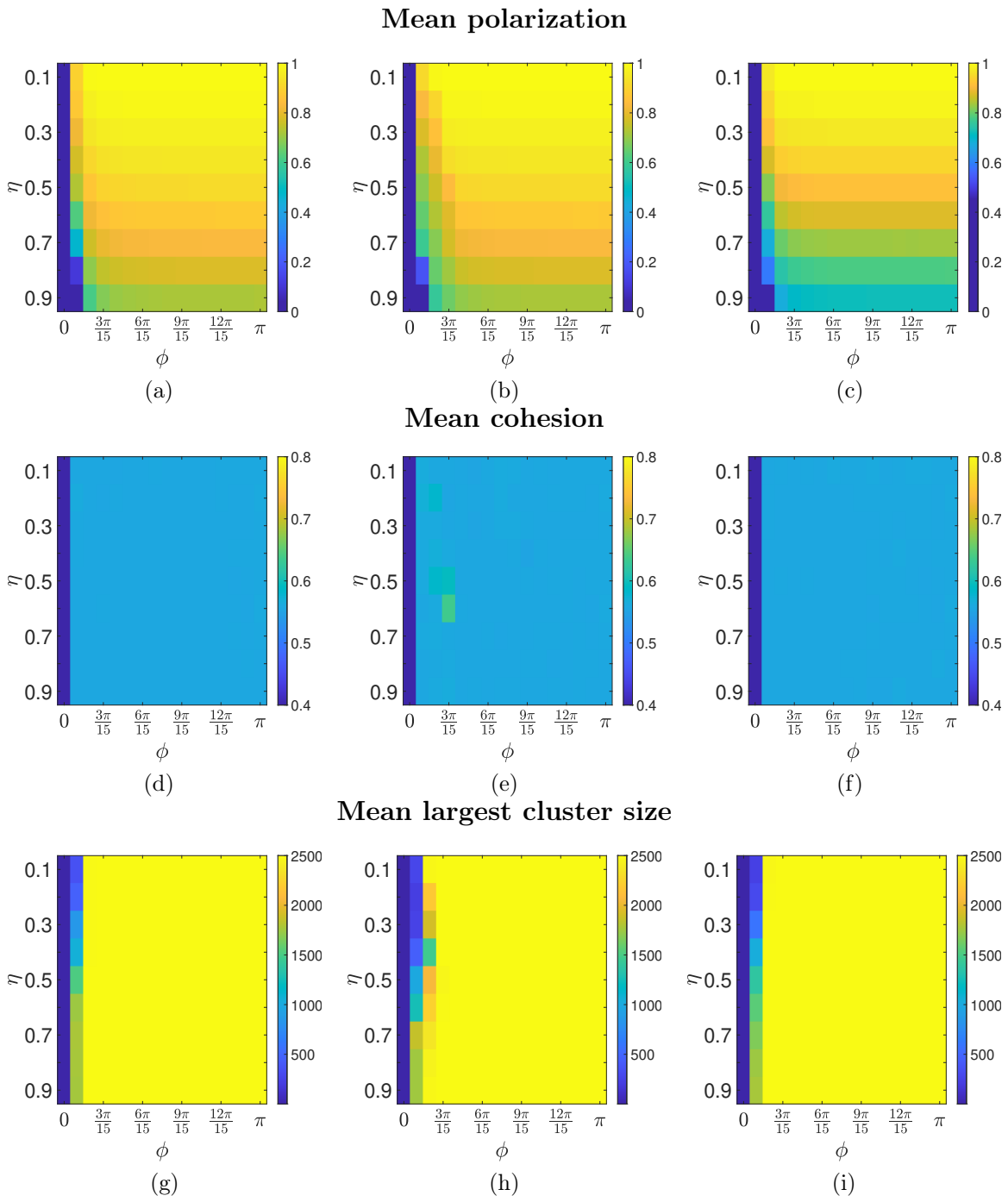

Figure 2-6: Order parameter results at $\rho = 20$ simulated for 2000 time steps. Mean polarization (top row), mean cohesion (middle row), mean largest cluster size (bottom row) are calculated for auditory (left column), visual (middle column), and composite sensing (right column) modes.

2.5 Conclusion

In this study, we introduce a three-dimensional collective motion model that integrates auditory and visual sensing modalities, inspired by species like bats that use these senses for effective navigation. The existing literature predominantly models sensing schemes similar to fields of vision, possibly due to an inherent human bias towards vision. However, there is substantial biological evidence indicating that many species utilize multiple sensory modalities. This work aims to examine the influence of combining sensing modalities on group behavior.

We explore the most generalized scenario of three-dimensional motion, a domain that has not been previously studied to combine sensory information. Through numerical simulations, we investigate the combined effects of auditory and visual sensing on group-level behavior, comparing them to the effects of pure vision and audition. The results reveal that composite sensing enables particles to interact with a larger set of neighbors, thereby accessing more information. This interaction facilitates the formation of a single, large, perfectly aligned group within a narrow sensing region—a feature achievable with pure vision only at a wider field of view. The findings of this study highlight the significant role that integrating information from multiple sensory modalities plays in emergent group-level behavior. These insights could have important applications in both biological and robotic swarms.

Future work will focus on several areas. Firstly, we will model the auditory and visual sensing sectors using biologically relevant and geometrically distinct parameters for r and ϕ. Secondly, we will implement differential weighting of information from the two sensory modalities to better understand their combined effects.

Chapter 3

The influence of visual field offset on collective behavior: an exploration using the two-dimensional Vicsek model

The content of this chapter is ready to be submitted for possible publication in a peer-reviewed journal.

3.1 Abstract

This study examines the effects of visual field offset on collective group behavior using the Vicsek model. Our results indicate that introducing an offset leads to a range of group behaviors, some of which are counter intuitive. Specifically, in the case of flipped sensing, where agents acquire information from behind their heading direction, we observe perfect group alignment and the entire group clustering at their center of mass, even under high noise conditions. This finding is in contrast to the typical properties of the Vicsek framework, where increased noise usually disrupts group behavior. Inspired by biological observations, where animals often utilize information outside their current heading, these findings offer valuable insights into the

advantages of such offset behaviors in natural systems and suggest applications in artificial systems.

3.2 Introduction

Collective behavior refers to the emergence of complex group-level patterns arising from the local interactions among individuals [1]. This phenomenon is evident in various biological systems, including bird flocks [14], fish schools [13], and insect colonies [19, 18, 91]. Such collective behaviors often confer advantages, such as improved predation [11], efficient foraging [12], information sharing [14, 15], reproductive success [16], and enhanced migration and defense strategies [17].

The efficiency of the group can be optimized through collective behavior, allowing organisms to perform tasks collectively or distribute the responsibilities of group survival through specialized roles [18, 12]. This is particularly apparent in the foraging strategies of insect colonies [19, 18], the migratory patterns of bird flocks and fish schools [17, 12], the hunting strategies of social predators like dolphins, orcas, wolves, and peregrine falcons [11, 16, 20], and the movement dynamics observed in elephant herds and muskoxen [21, 22].

Various models have been developed to study collective behavior, ranging from continuous differential equations to discrete-time agent-based models [1]. Agent-based modeling has become a popular tool for studying group behavior using computer simulations. It allows each agent is specified simple rules or behaviors of interaction, often leading to various distinct group behavior similar to that we see in nature[92]. A popular agent-based model for studying collective behavior is the Vicsek model, renowned for its minimalistic approach. In the original Vicsek model, agents move at a constant speed in a two-dimensional domain, aligning with the average direction of their neighbors while incorporating some noise. Each agent has a circular sensing region, and its neighbors are those within this region, including itself [2].

Due to its simplicity, the Vicsek model has inspired various modifications, such as the inclusion of attractive and repulsive interactions [40], extensions to three dimen-

sions [70], and biologically-inspired sensing modes [3, 93]. Additionally, the model has been applied to financial markets [94] and hydrostatics [95]. Inspired from nature that animals using visual sensing modes with limited fields of view, some studies limit the agent's sensing range to a sector instead of the full circular range [71, 45, 3, 93]. However these models assume that the sensing sector is symmetric to the agent's heading direction. However, empirical evidence suggests that there may be advantages to having the sensing region offset from the direction of travel. Evolutionary adaptations, such as saccadic head movements in blowflies and lateral scanning in locusts, are used to establish gaze and measure distance for locomotion [96].

While it may seem counter-intuitive for an animal to look in a direction independent of its movement, many animals scan areas outside their heading to gather spatial information and inform response maneuvers through selective attention and dynamic sensory loads [20, 97]. A fascinating example is bottlenose dolphins, which direct their sonar beams slightly off-axis when locating and tracking a target [98]. Models that consider sensing sectors offset from an individual's heading direction are lacking in the literature, but there are strong incentives to such potential insight such as informing sensor placement and reducing information obstruction [99, 100, 101].

Studying collective behavior in animals provides valuable insights into the natural world and motivates practical applications in engineered systems, particularly bio-inspired multi-robot teams [102, 103]. Understanding how complex coordination is achieved without centralized control in nature can inspire more effective control systems and algorithms, leading to improved engineering designs [103, 50, 51, 52], such as the development of target tracking and swarming maneuvers for autonomous drones in a militaristic setting [104, 105]. In this context, investigating the impact of offset on group-level behavior may drive technological advancements.

In this paper, the original Vicsek model is modified to have a variable-width sensing sector whose axis of symmetry is offset from the heading of the agent. Simulations are conducted to investigate how this change in the direction of sensing affects the emergent group behaviour, quantified by well-defined order parameters.

3.3 Modeling

3.3.1 System dynamics

Here we consider a modified version of the original Vicsek model where the agents implement the use of a sector field-of-view, and the center of this sector is shifted by some angle α from the agent's heading. The neighbors of each agent are those that exist within that sector field of view. The update protocol is the same as in the original Vicsek model, i.e. the heading is updated as the average resultant direction of the neighbors. Each agent is modelled as having a sensing region akin to a field-of-view. This region is modelled as a sector defined by a radius of length r and a central angle 2ϕ, where ϕ denotes the *sensing angle*. The sensing angle lies within the range $[0, \pi]$ and is symmetrical on either side of the sector centered around the axis of the agent's heading plus the offset α. Notice that when the sensing angle $\phi = \pi$, the interaction neighborhood is a full circle, regardless of offset α. The model is then essentially reduced to the regular original Vicsek model.

The original two-dimensional (2D) Vicsek model is a popular agent-based framework for studying collective behavior and pattern formation in systems of self-propelled particles. In this model, each particle moves with a constant speed in a two-dimensional space. In the original Vicsek model, the neighbors of a particle are defined as all particles within a specified radius, known as the sensing radius. Specifically, at each time step, the direction of each particle is updated to align with the average direction of all particles within its sensing radius, while incorporating some random noise. The update rule for the heading direction θ_i of particle i at time $t + \Delta t$ is given by:

$$\theta_i(t + \Delta t) = \langle \theta_j(t) \rangle_R + \eta \xi_i(t), \tag{3.1}$$

where $\langle \theta_j(t) \rangle_R$ represents the average direction of all particles j within the sensing radius R of particle i, η is the noise intensity, and $\xi_i(t)$ is a random variable uniformly distributed in $[-1, 1]$. Each particle then updates its position according to its new

direction:

$$\mathbf{r}_i(t + \Delta t) = \mathbf{r}_i(t) + v_0 \mathbf{v}_i(t)\Delta t, \tag{3.2}$$

where $\mathbf{r}_i(t)$ is the position of particle i at time t, v_0 is the constant speed, $\mathbf{v}_i(t)$ is the unit velocity vector of particle i determined by its direction $\theta_i(t)$, and $\Delta t = 1$.

The Vicsek model is notable for its simplicity and ability to reproduce a range of complex collective behaviors, such as flocking and swarming, through local interaction rules. This model has been the basis for numerous studies and modifications, making it a fundamental tool in the exploration of collective dynamics in biological and artificial systems.

3.3.2 Offset sensing

In this study, we consider a modified version of the original Vicsek model, where agents use a sector instead of a complete circle as their sensing region to detect neighbors, effectively implementing a field of vision. Specifically, the field of view is modeled as a sector defined by a radius r and an opening angle 2ϕ, where ϕ represents the *sensing angle*. To create an offset field of view, we introduce another angle α, which is the angle between the center of this sector and the agent's current heading direction. For a fixed offset α, the sensing angle is constructed symmetrically around the offset angle. Figure 3-1 presents a schematic explaining the implementation of the offset field of view.

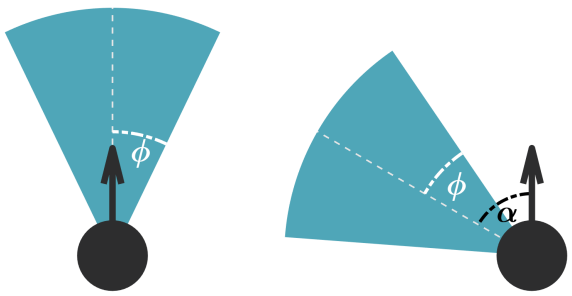

Figure 3-1: Schematic of the implementation of the offset. (a) Without an offset, where the offset angle $\alpha = 0$. (b) With an offset, where the offset angle $\alpha \neq 0$. The sectors have an opening angle of 2ϕ, where ϕ is the sensing angle.

Each agent uses this sector-shaped sensing region to identify neighbors, which are those agents located within its field of view. Once neighbors are determined, the position and direction update protocols (equations 3.1 and 3.2) remain the same as in the original Vicsek model.

For the simulations, we consider different values of the sensing angle ϕ within the range $[0, \pi]$. When the sensing angle $\phi = \pi$, the interaction neighborhood forms a full circle, similar to the original Vicsek model, regardless of the offset α.

3.3.3 Order parameters

To analyze the collective behavior of the system, we utilize order parameters such as polarization, cohesion, cluster size, and coverage.

Polarization is a measure of the alignment of all agents in the system. It is defined as the magnitude of the average velocity vector of all agents, normalized by the number of agents. Specifically, it is given by:

$$P(t) = \frac{1}{N} \left| \sum_{i=1}^{N} \mathbf{v}_i(t) \right|, \tag{3.3}$$

where N is the total number of agents, $|\cdot|$ denotes the norm of the vector, and $\mathbf{v}_i(t)$ is the unit velocity vector of the i-th agent at time t. A polarization value of one indicates perfect group alignment, while a value close to zero indicates random orientations.

Cohesion quantifies the degree to which agents are grouped together. It is typically defined as a scaled function of the average distance between each agent and the center of mass of the group. Cohesion C is written as:

$$C(t) = \frac{1}{N} \sum_{i=1}^{N} \exp \left[- \frac{\left| \mathbf{r}_i(t) - \mathbf{r}_{\mathrm{cm}(t)} \right|}{l_a} \right],$$

where $\mathbf{r}_i$ is the position of the i-th agent, and $\mathbf{r}_{\mathrm{cm}}$ is the center of mass of the group. We use the scaling coefficient $l_a = 4R$, following the study by [64]. Cohesion ranges from zero to one, and higher values indicate a more tightly packed group.

Largest cluster size refers to the size of the largest weakly connected group of agents. In a group of N agents, the largest possible cluster size is the total number of agents, where all agents are weakly connected through their neighbors.

Coverage measures the spatial distribution of agents across the domain. It is defined as the time-averaged fraction of the area occupied by agents. The domain is divided into a grid, and the normalized mean number of times each grid cell is occupied is computed. This gives an idea of how uniformly the agents are spread across the space. High coverage values indicate that agents are well dispersed within the domain.

Evaluating these order parameters provides a comprehensive understanding of the system's collective dynamics and spatial organization.

3.4 Results and discussion

We perform simulations across a broad range of parameters to analyze the group-level behaviors. Specifically, we vary the noise parameter, η, and the sensing half-angle, ϕ, under different offset configurations by adjusting α. This allows us to study group-level behaviors in terms of the previously defined order parameters. For our simulations, we consider a square arena with side length $L = 10$, assuming periodic boundary conditions similar to those in the original Vicsek model. Simulations are conducted for 5000 time steps, with the first 1000 time steps discarded to eliminate any effect from transient. We assume a constant speed of $v_0 = 0.03$ and a constant sensing radius of $R = 1$ for all agents at all times. All agents are initialized with random positions and headings, within the square domain and the unit circle, respectively, using uniform distributions. We generate the initial conditions once and use the same conditions in all simulations. The density is set to $\rho = 8$, resulting in $N = 800$ agents.

Before examining the results of the order parameters, we present snapshots of simulations in Figure 3-2 for various offset angles α at time $t = 5000$, with noise intensity $\eta = 0.8$ and sensing angle $\phi = 5\pi/15$. For these snapshots, the parameters

η and ϕ are arbitrarily chosen, and the offset field of view is varied from $\alpha = 0$ to $\alpha = 11\pi/6$ radians in increments of $\pi/6$ radians. Note that $\alpha = 0$ is equivalent to $\alpha = 2\pi$, both indicating no offset and therefore, we only present $\alpha = 0$.

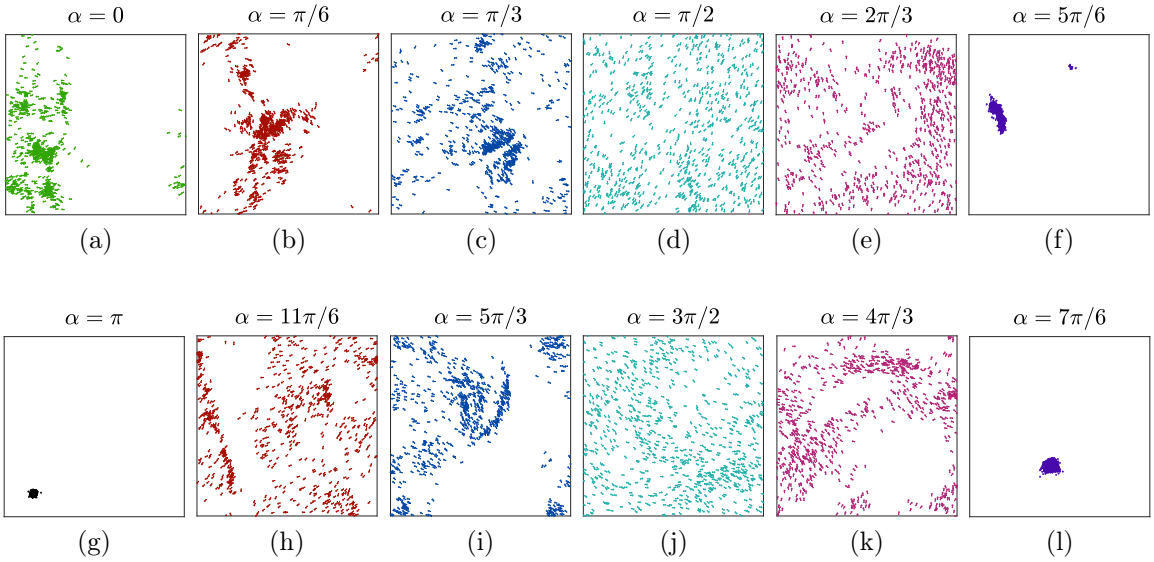

Figure 3-2: Snapshots of simulations for various offset angles α at time $t = 5000$, with parameters $\eta = 0.8$ and $\phi = \frac{5\pi}{15}$.

Comparing the sub-figures in Figure 3-2, we observe distinct group behaviors in terms of alignment and cohesion as the offset angle varies. For example, at $\alpha = \pi/2$ and $\alpha = 3\pi/2$, the agents are more spread out, occupying the entire simulation arena. In contrast, at $\alpha = 5\pi/6$, $\alpha = \pi$, and $\alpha = 7\pi/6$, the groups display closely packed clusters.

Next, we vary the control parameters, which include the noise intensity η, the sensing angle ϕ, and the offset angle α, and compute the mean polarization, mean cohesion, and mean largest cluster size values. The mean values are computed by taking an average over 4000 time steps and are presented in Figures 3-3 to 3-5. In each sub-figure, we vary η from 0 to 0.9 in increments of 0.1, and ϕ from 0 to π in increments of $\pi/15$ radians. Additionally, we explore different values of α ranging from 0 to 2π in increments of $\pi/6$ radians. We present the results for increasing α, considering its symmetry. For instance, $\alpha = \pi/6$ means a $\pi/6$ radians offset to the left of the heading direction, while $\alpha = 11\pi/6$ means same $\pi/6$ radians offset but to the right of the heading. To maintain symmetry, we arrange the sub-figures 3-3h to

3-3l so that after $\alpha = \pi$, the sequence starts matching the sequence of increasing α from $\pi/6$ to $5\pi/6$ as in sub-figures 3-3a to 3-3f.

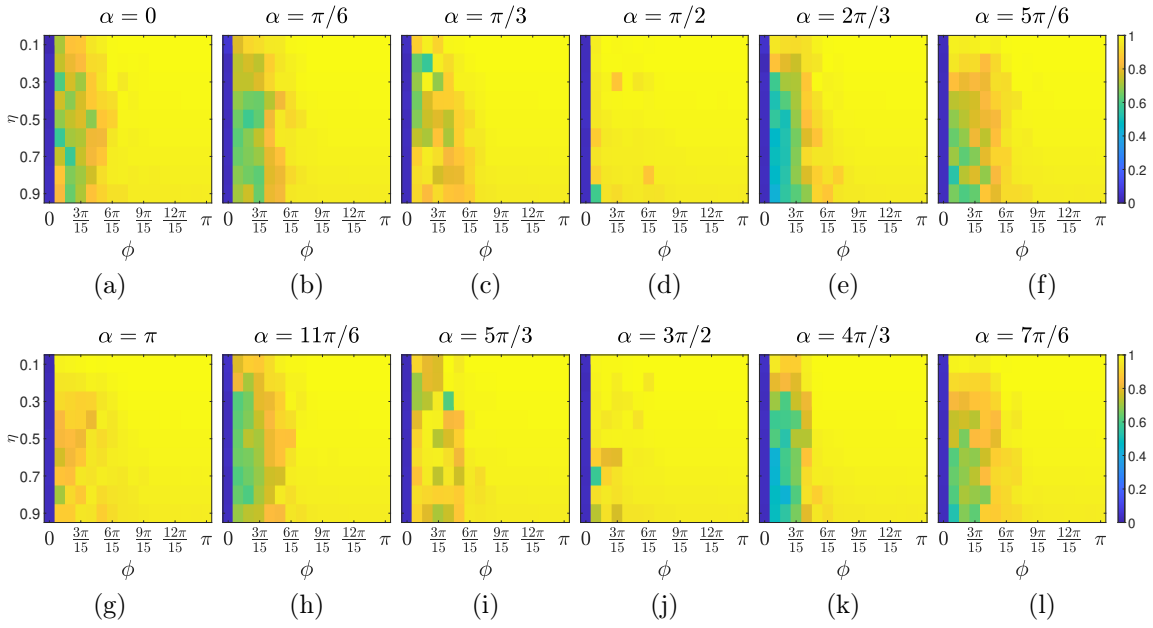

Figure 3-3: Results for mean polarization at varying noise intensity η and sensing angle ϕ for different offset angles α.

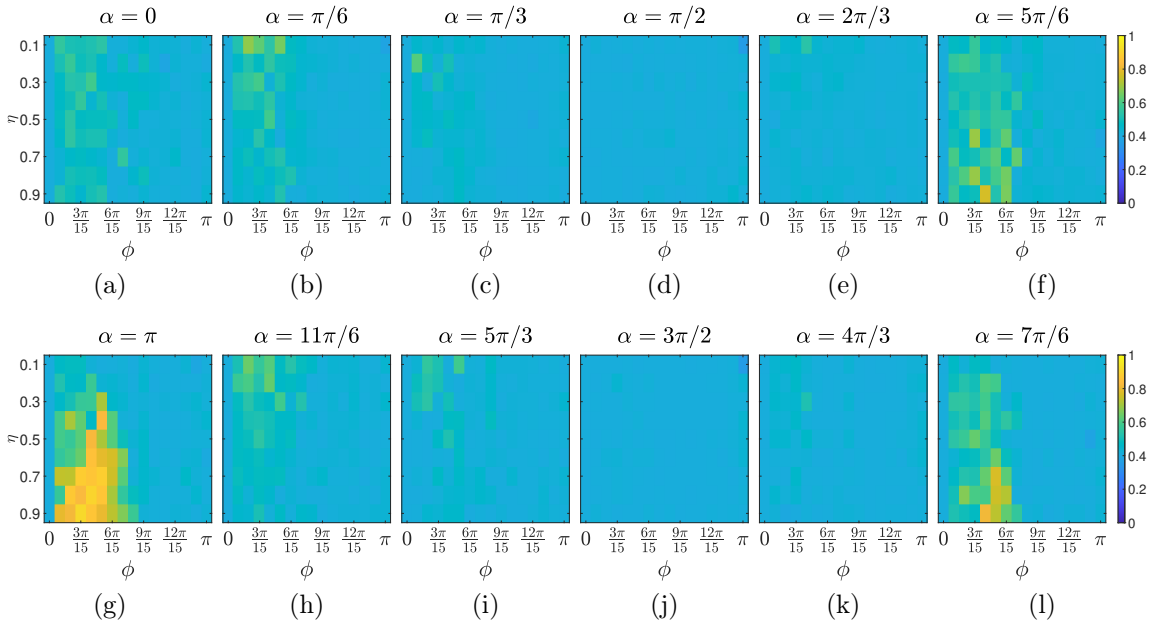

Figure 3-4: Results for mean cohesion at varying noise intensity η and sensing angle ϕ for different offset angles α.

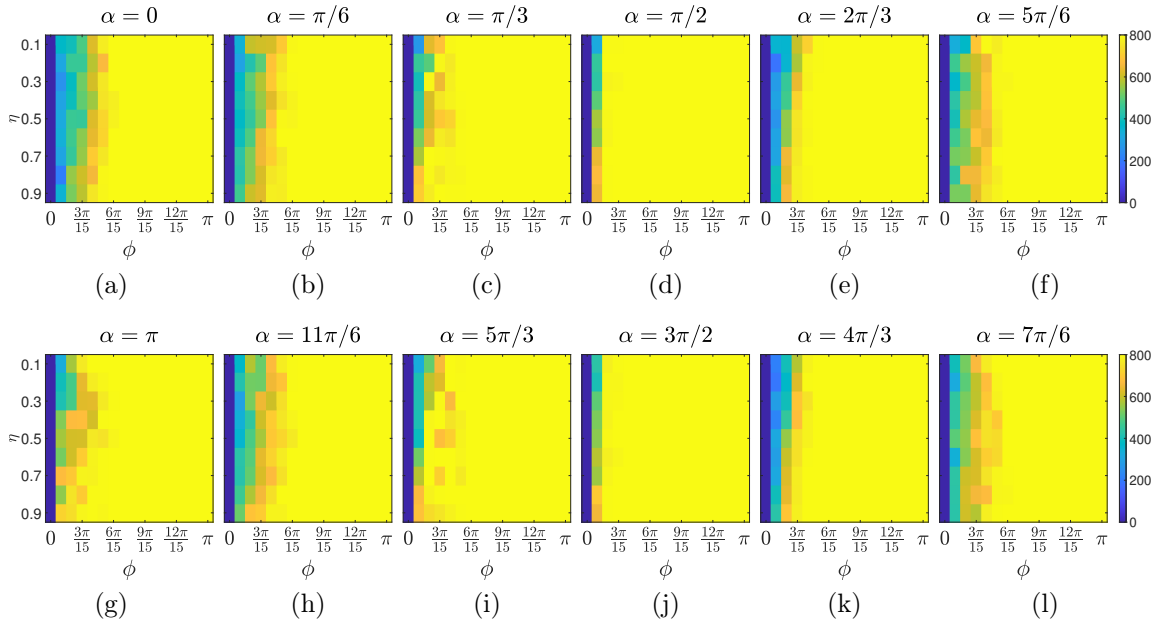

Figure 3-5: Results for mean largest cluster size at varying noise intensity η and sensing angle ϕ for different offset angles α.

In Figure 3-3, each sub-figure shows that the mean polarization values are zero when the sensing angle $\phi = 0$, and the polarization reaches one when $\phi = \pi$. Notably, $\phi = 0$ indicates that agents lack a sensing region, resulting in no interaction with neighbors and consequently a random walk behavior. Conversely, when $\phi = \pi$, the sensing region forms a complete circle, similar to the original Vicsek model, regardless of the different values of α.

Interestingly, we observe variations in group behavior, as indicated by polarization, cohesion, and largest cluster size, across different values of α. Starting with polarization in Figure 3-3, we observe that polarization values reach one, indicating perfect group alignment, when the sensing angles are relatively large ($\phi \geq 8\pi/15$) for all values of α. Smaller polarization values are observed with smaller sensing angles, although this depends on the offset angle. Specifically, with a small sensing angle, polarization is low when there is no offset ($\alpha = 0$), gradually increasing as α increases, peaking at $\alpha = \pi/2$, and then decreasing again, with a slight improvement at $\alpha = \pi$. Additionally, at small sensing angles, the polarization values are symmetric with respect to α, indicating that the behavior does not depend on whether the offset is to

the right or left of the heading direction. For example, due to the symmetric nature, the high polarization observed at $\alpha = \pi/2$ is also present at $\alpha = 3\pi/2$ configuration. For some fixed values of α, we observe that polarization values are sensitive to noise at small sensing angles. For example, polarization decreases as noise increases, as illustrated in Figures 3-3e, 3-3f, 3-3g, 3-3k, and 3-3l, for fixed α values of $2\pi/3$, $5\pi/6$, π, $4\pi/3$, and $7\pi/6$, respectively.

Differences in group behavior are also evident in terms of cohesion for various offset values, as illustrated in Figure 3-4. The cohesion of a group is symmetrical with respect to the offset angle, indicating that group behavior is not dependent on whether the offset is left or right of heading. Similar to polarization, the differences with respect to α emerge at small sensing angles. However, unlike polarization, cohesion is high in the absence of offset (Figure 3-4a), then gradually decreases to a minimum at $\alpha = \pi/2$ (Figure 3-4d), and subsequently increases with further increments in α. The highest cohesion at small sensing angles is observed at $\alpha = \pi$ (Figure 3-4g), and interestingly, this peak occurs at the high noise intensity. In contrast to the polarization results, we observe that cohesion values increase with increasing noise for fixed values of α. This behavior is evident in Figures 3-4f, 3-4g, and 3-4l, for fixed α values of $5\pi/6$, π, and $7\pi/6$, respectively. This result is counter intuitive, as group behaviors are generally expected to deteriorate with increasing noise. However, here we observe that group behavior, specifically cohesion, improves with increased noise.

Next, we focus on the largest cluster size, which is determined by the number of agents in the system, set to $N = 800$ for our simulation parameters. As shown in Figure 3-5, the largest cluster size exhibits symmetry across offset angles. Similar to polarization and cohesion, differences in the largest cluster size are only noted at small sensing angles. Initially, at small sensing angles, the largest cluster size is small in the absence of an offset (Figure 3-5a) and improves with increasing offset, reaching a maximum at $\alpha = \pi/2$ (Figure 3-5d) and at the symmetric configuration of $\alpha = 3\pi/2$ (Figure 3-5j), before decreasing again. Interestingly, the largest cluster size is sensitive to noise but counter intuitively increases with noise. This behavior is observed in Figures 3-5d, 3-5e, 3-5g, 3-5j, and 3-5k.

Combining all the order parameter results, we observe interesting behaviors at small sensing angles. For an offset angle of $\alpha = \pi/2$ (and the symmetric configuration of $3\pi/2$), the entire group moves together with a common heading direction, resulting in polarization values reaching the maximum of one and the agents form one large cluster. However, the group is uniformly dispersed within the simulated arena, reducing overall cohesion. This is supported by the visualization in Figures 3-2d and 3-2j Even more intriguing and counter intuitive results are observed at small sensing angles when the offset angle is $\alpha = \pi$ and noise intensity is high. In this scenario, not only does polarization reach its maximum possible value of one, but cohesion is close to its maximum value of one, and the largest cluster size is also very high. Figure 3-2g shows the corresponding formation of a singular dense cluster of highly aligned agents.

To verify that agents are uniformly dispersed within the simulated arena based on low cohesion, we compute the order parameter coverage, which is the time-averaged fraction of area occupied by the agents within the domain. We calculate mean coverage in the same manner as the mean values for the other order parameters. Figure 3-6 presents the mean coverage.

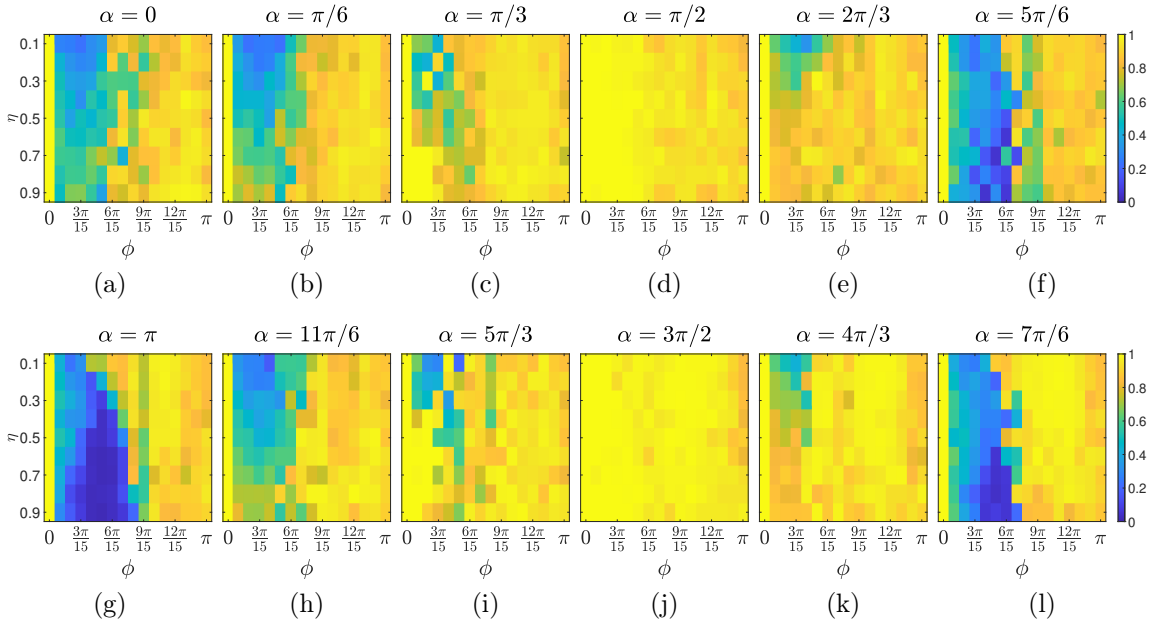

Figure 3-6: Results for mean coverage at varying noise intensity η and sensing angle ϕ for different offset angles α.

Results show that coverage is highly correlated with the inverse of cohesion, as shown in Figure 3-4. The symmetry observed around the offset of $\alpha = \pi$ confirms that spatial distributions do not depend on the direction of the offset from the heading direction. The highest coverage across all noise and sensing angles is observed for offset angle $\alpha = \pi/2$ and $\alpha = 3\pi/2$, where we previously noted low cohesion, high polarization, and single cluster formation. These results indicate that all the agents are uniformly spread within the domain while achieving perfect alignment as a group. The lowest coverage, on the other hand, is observed at high noise and small sensing angles for an offset angle of $\alpha = \pi$, where we previously observed the counter intuitive result of high cohesion. Specifically, a cohesion value close to one indicates that all the agents collapse at their center of mass. When compared with the coverage results, which are close to zero, this confirms that the group is very tightly packed.

3.4.1 Flipped sensing

To further investigate the intriguing case of $\alpha = \pi$, which we refer to as flipped sensing, we conduct a new set of simulations with noise intensity varied over a larger range. The results are presented in Figure 3-7. We also compare the results of the flipped sensing to those obtained in the absence of an offset. Sub-figures 3-7a and 3-7b show the mean polarization, while sub-figures 3-7c and 3-7d show the mean cohesion. The results with no offset are indicated by $\alpha = 0$, while the results for flipped sensing are indicaed by $\alpha = \pi$.

Comparing the polarization results, we observe that flipped sensing leads to higher polarization at smaller sensing angles for higher noise values, before transitioning to random walk behavior when noise levels become too high. For instance, at $\phi = \pi/15$, random walk behavior begins at approximately $\eta = 2$ in the absence of offset, whereas with flipped sensing, it starts at $\eta = 4$ for the same sensing angle. Additionally, we observe that polarization improves with increasing sensing angle for a fixed noise level in the case of no offset. Interestingly, in the case of flipped sensing, this is not observed. At high noise levels, polarization initially increases with the sensing angle, then decreases again as the sensing angle is further increased.

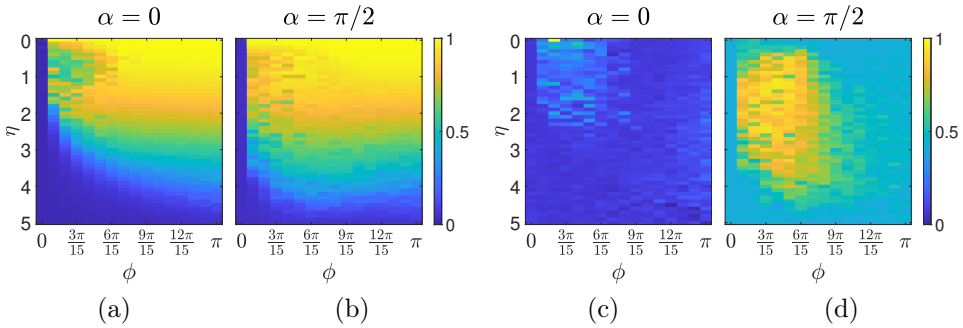

Figure 3-7: Mean polarization ((a) and (b)) and mean cohesion ((c) and (d)) are computed for a larger range of $\eta : [0, 5]$ with varying $\phi : [0, \pi]$. Sub-figures (a) and (c) show results with no offset, while sub-figures (b) and (d) show results with a flipped sensing, i.e., offset of $\alpha = \pi$.

Notable differences are also observed in the mean cohesion values when comparing high noise levels. Flipped sensing demonstrates very high cohesion with increasing noise for a small range of sensing angles, but then cohesion decreases when noise $\eta \geq 4$. When compared with the polarization results in flipped sensing, we already observe an increase in polarization with increasing sensing angle (from $3\pi/15$ to $6\pi/15$) for large noise values, which also corresponds to regions of high cohesion. These results when combined indicate that the differences in sensing between no offset and π offset create variations in interaction that influence group behavior by increasing cohesion in flipped sensing. This high cohesion eventually helps the group maintain moderate polarization, a phenomenon not observed in the no offset case where both cohesion and polarization remain low.

3.4.2 Additional investigations

Several supplementary investigations are done to study flipped sensing further. I an attempt to explain the group-level emergent behavior, the pairwise interactions and the number of unique neighbors between the agents are compared for the no offset model and the flipped sensing model. The informative, but surprisingly, counter-intuitive results observed further motivate the need for future research into the flipped sensing and models with an offset sensing as a whole.

Difference of closest approach - pairwise interaction

It is known and verified that the average particle density is a driving factor for the emergent behavior in the Vicsek model [2, 1, 24]. Increasing density leads to increased interaction between agents, thus, it is beneficial to investigate the pairwise interactions between agents [3, 38, 106].

A pair of agents are simulated with initial positions $x_1^0 = \left[\begin{smallmatrix} 0 \\ -2.25 \end{smallmatrix}\right]$ and $x_2^0 = \left[\begin{smallmatrix} 5 \\ 0 \end{smallmatrix}\right]$ and initial direction of the first agent as $\theta_1^0 = \frac{\pi}{2}$. The initial heading of the second agent, θ_2^0, and sensing angle, ϕ, are varied and the interactions are simulated for the regular and flipped case. The set-up is shown in Figure 3-8.

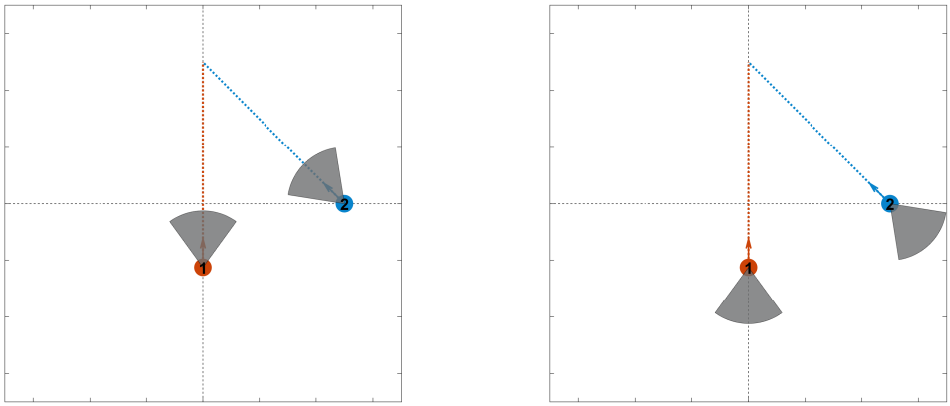

(a) (b)

Figure 3-8: Domain arrangement for Pairwise Interaction between two agents when $\alpha = 0$ (3-8a) and $\alpha = \pi$ (3-8b). For this example $\theta_2^0 = \frac{3\pi}{4}$ and $\phi = \frac{3\pi}{15}$. The radius of the sensing sector is exaggerated for visualization purposes. The dotted lines show the paths of the agents without interaction.

The distance of closest approach is calculated in each case. The differences between those distances are computed and shown in Figure 3-9. In order for the results to be untainted by randomness and to ensure controllability of the trajectories, the simulation is run without any noise $\eta = 0$.

The flipped sensing maintains a higher distance for $\phi : [\frac{\pi}{15}, \frac{7\pi}{15}]$. Special cases exist at $\left(\phi = \frac{6\pi}{15}, \theta_2 = \frac{31\pi}{40}\right)$, $\left(\phi = \frac{7\pi}{15}, \theta_2 = \frac{[30,31,32]}{40}\pi\right)$, $\left(\phi = \frac{8\pi}{15}, \theta_2 = \frac{[30,31,32]}{40}\pi\right)$, and $\left(\phi = \frac{9\pi}{15}, \theta_2 = \frac{31\pi}{40}\right)$, where the flipped sensing has a smaller separation distance when

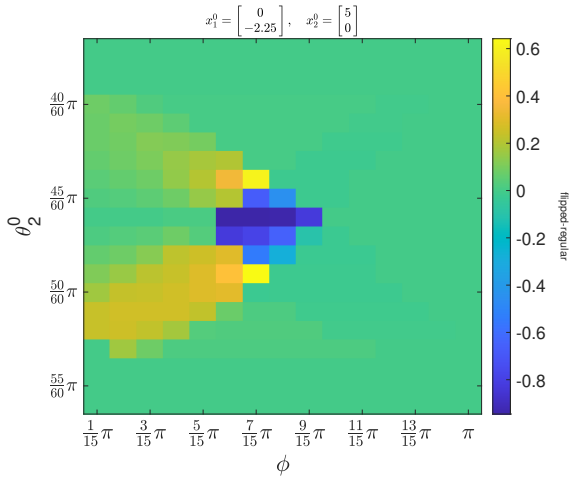

Figure 3-9: Difference of Distances of Closest Approach: Flipped-Regular. Positive value indicates a flipped sensing has a higher distance of closest approach relative to regular sensing, and vice-versa.

compared to the no offset case.

The distances of closest approach may be related to cohesion in the group-level behavior. Therefore, lower distances of closest approach may be expected indicate higher cohesion, and vice-versa. Relating Figure 3-9 and Figure 3-4, the darker regions on Figure 3-9 should indicate higher cohesion on Figure 3-4. This is not the case as the cohesion for both regular and flipped sensing are low and equivalent at the queried ϕ values $\left(\left[\frac{6\pi}{15}, \frac{9\pi}{15}\right]\right)$, at the $\eta = 0$ case. It is only when η is increased past $\eta = 0.4$ that the flipped sensing shows higher cohesion than in the regular case.

Mean difference of closest approach – circular arrangement

In the previous analysis, interaction between the pair of agents is not guaranteed, hence a lot of the data points are of little use. A new analysis is done where $N = 11$ agents are arranged in a circular topography around the center of the arena, with initial headings pointing towards the center, as depicted in Figure 3-10.

This arrangement forces interaction, allows for the inclusion of more agents, and allows for the dynamics of agent decision-making in a cluster to be explored. The distance of closest approach of all agents with each other is calculated, and the mean of these values is computed. This is done for $\eta : [0, 5]$, and $\phi : [0, \pi]$ in increments

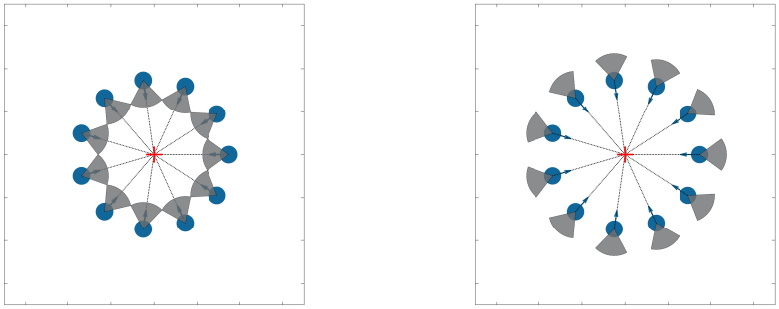

(a) (b)

Figure 3-10: Domain configuration for interaction of 11 agents in circular arrangement when $\alpha = 0$ (3-10a) and $\alpha = \pi$ (3-10b). For this example $\phi = \frac{3\pi}{15}$. The radius of the sensing sector is exaggerated for visualization purposes. The dotted lines show the paths of the agents without interaction.

of $\frac{\pi}{15}$. Figure 3-11 shows the mean difference of distance of closest approach between the flipped sensing case and the no offset case.

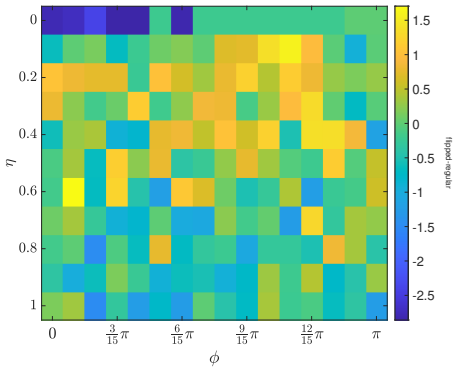

Figure 3-11: Mean Difference of Distances of Closest Approach: Flipped-Regular, Circular Arrangement. Positive value indicates a flipped sensing has a higher distance of closest approach relative to regular sensing, and vice-versa.

Agents in the flipped sensing generally maintain a higher distance for $\eta \leq 0.3$, especially in the range $\phi : \left[\frac{8\pi}{15}, \frac{12\pi}{15}\right]$. At $\eta = 0.2$, there is higher separation in flipped sensing, occurring at lower sensing angles as well $\left(\phi : \left[0, \frac{3\pi}{15}\right]\right)$. For the deterministic case $(\eta = 0)$, regular sensing has higher separation distance for $\phi : \left[0, \frac{4\pi}{15}\right]$. In all other cases, the differences between the two cases are zero or negligible. For these ranges where the flipped sensing maintains a higher separation distance, the associated cohesion values from Figure 3-4 are low. For the η range, the cohesion is low,

but as noise increases, the cohesion is especially in the range $\phi : \left[\frac{3\pi}{15}, \frac{6\pi}{15}\right]$.

Mean number of unique neighbors

Figure 3-12 shows the mean number of unique neighbors for the no offset ($\alpha = 0$) and flipped ($\alpha = \pi$) cases. This analysis case consisted of $N = 11$ agents arranged in a circular distribution about the center of the domain - the same as depicted in Figure 3-10. The results shown depict the average of five independent simulations. These results indicate that the agents generally have more neighbors in the regular ($\alpha = 0$) case when compared to the flipped case, with the only exception being when $\eta = 0$ and $\phi \leq 7\pi/15$. Disregarding $\phi = \pi$, the flipped sensing case only has a relatively high number of neighbors when there is no noise, i.e. $\eta = 0$. This is counter-intuitive as it has been previously observed that there is both high polarisation and cohesion in the flipped case at high noise levels, at least for $\eta : [0, 2.3]$. What does agree with previous observations is that agents in the flipped sensing are able to have higher neighbor interactions at lower sensing angles ϕ. Although these high interactions only occur in the $\eta = 0$ case, the results do concur with previously observed trends relating to sensing angle ϕ.

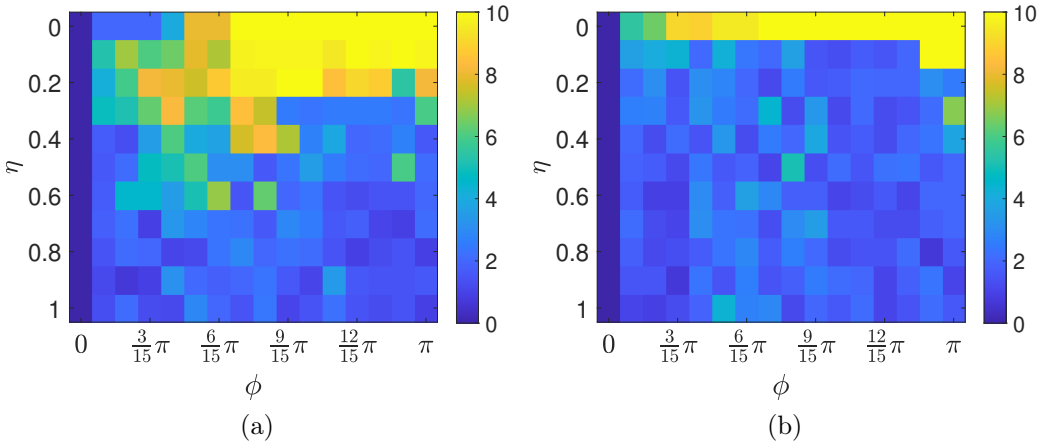

Figure 3-12: Comparison of mean number of unique neighbors between the no offset (3-12a) and flipped (3-12b) models for $\eta : [0 : 1]$. The average number of unique neighbors is computed over 5 trials.

3.5 Conclusion

This study investigates the impact of visual field offset on group collective behavior using the Vicsek model. Our findings reveal that introducing an offset generates a variety of group behaviors, some of which are counter-intuitive. Notably, in the scenario of flipped sensing, which creates an offset of π radians, we observe perfect group alignment and the entire group clustering at their center of mass, even under high noise conditions. This result contrasts with the traditional properties of the Vicsek framework, where increasing noise typically deteriorates group behavior.

These findings are inspired by biological observations, where animals often use information outside of their current heading. The results are significant as they provide insights into the potential advantages of such offset behaviors in natural systems and offer inspiration for designing artificial systems. For instance, this study suggests that incorporating offset sensing in multi-robot teams could achieve desired group behaviors.

Future work will extend this investigation to a three-dimensional Vicsek model with offset, reflecting more natural systems that navigate in three-dimensional environments. Additionally, rather than keeping the offset fixed for a given simulation, it would be intriguing to explore the effects of dynamic offsets that change over time, potentially leading to more complex behaviors. This initial exploration of offset visual fields opens numerous exciting questions for researchers interested in studying collective motion.

Chapter 4

Overall Conclusion and Future Work

In this thesis, we investigated the effects of bio-inspired sensing mechanisms on collective behavior using modified versions of the Vicsek model. We developed a three-dimensional collective motion model that integrates auditory and visual sensing modalities, inspired by species like bats that utilize these senses for effective navigation. Existing literature predominantly focuses on sensing schemes akin to fields of vision, likely due to an inherent human bias towards vision. However, substantial biological evidence indicates that many species employ multiple sensory modalities. This research aims to explore the influence of combined sensing modalities on group behavior.

Through numerical simulations, we examined the combined effects of auditory and visual sensing on group-level behavior, comparing them to the effects of pure vision and audition. The results demonstrated that composite sensing enables particles to interact with a larger set of neighbors, thereby accessing more information. This interaction facilitates the formation of a single, large, perfectly aligned group within a narrow sensing region—a feature achievable with pure vision only at a wider field of view. These findings underscore the significant role of integrating information from multiple sensory modalities in shaping emergent group-level behavior, with important implications for both biological studies and the development of robotic swarms.

Furthermore, we explored the impact of visual field offset on group collective behavior using the Vicsek model. Our findings indicated that introducing an offset

generates a variety of group behaviors, some of which are counter intuitive. Notably, in the scenario of flipped sensing, we observed perfect group alignment and the entire group clustering at their center of mass, even under high noise conditions. This result contrasts with the traditional properties of the Vicsek framework, where increasing noise typically deteriorates group behavior. Inspired by biological observations where animals often use information outside their current heading, these findings provide insights into the potential advantages of such offset behaviors in natural systems and offer inspiration for designing artificial systems. For instance, incorporating offset sensing in multi-robot teams could help achieve desired group behaviors.

The investigation and use of different sensing mechanisms in collective behavior modelling can have transferable advantages to real-world systems. For example, the combination of auditory and visual sensing can be applied to sensor fusion in autonomous vehicles for resilient collision detection and path planning, while the offset sensing can be analogous to an entity's selective attention to certain directional signals or choosing specific crucial information.

Future work will focus on several areas. Firstly, we will model the auditory and visual sensing sectors using biologically relevant and geometrically distinct parameters for sensing radius and sensing angle. Secondly, we will implement differential weighting of information from the two sensory modalities to better understand their combined effects. Additionally, we will extend the investigation to a three-dimensional Vicsek model with offset, reflecting more natural systems that navigate in three-dimensional environments. Exploring the effects of dynamic offsets that change over time will also be intriguing, potentially leading to more complex behaviors. This initial exploration of offset visual fields opens numerous exciting questions for researchers interested in studying collective motion.

Appendix A

MATLAB Codes

Presented are simplified versions the MATLAB codes used to conduct the work done in this thesis. The scripts and methods were optimized to use less memory for computation through vectorization principles. For example, a single adjacency matrix was used to represent the neighbors of all the agents at any given time. All work was done on either a personal computer or using the resources provided by the Complex Dynamical Systems Laboratory at Embry-Riddle Aeronautical University - Daytona Beach. In several instances, parallel computing resources, via the VEGA HPC housed at ERAU, were utilized to aid in computation time and facilitate the analysis of denser systems.

A.1 3D Vicsek model

```
function [posAll,eVecAll,DD] = vicsek3d(N,simTime,dt,roi,phi,eta,v0,
    initialPosition,initialOrientationAngles,Domain,typeBC,mode)

% Initialise all Particles with random positions, orientations, and
    initial velocity within the grid
pos = initialPosition;
theta = initialOrientationAngles(1,:);
zeta = initialOrientationAngles(2,:);
u = cos(zeta);
eVec = [sqrt(1-u.^2).*cos(theta); sqrt(1-u.^2).*sin(theta); u]; %
    heading or direction of movement of particle

% Analysis and Simulation
DD = cell(simTime,1);
posAll = zeros(3,N,simTime);
eVecAll = zeros(3,N,simTime);

for k = 1:dt:simTime
    posAll(:,:,k) = pos;
    eVecAll(:,:,k) = eVec;
    DD{k} = determineNeighbours(mode,pos,eVec,roi,phi,Domain,typeBC)
    ;
    [pos,eVec] = determineNewParams(DD{k},pos,eVec,v0,eta,Domain,
    typeBC,dt);
end

end

%FUNCTIONS
function [adjacency] = determineNeighbours(mode,pos,eVec,roi,phi,
    Domain,typeBC)
% for each particle, if a surrounding particle is within sensing
% region, then that particle is considered a neighbour
N = size(pos,2);
```

```
logical allisNeighbour;
allisNeighbour = false(N);

for i=1:N
    resVec = pos-pos(:,i); %vectors from ith particle to all other
   particles
    if typeBC == "Periodic"
        resVec = mod(resVec+(Domain(:,2)-Domain(:,1) )/2, Domain
   (:,2)-Domain(:,1) ) - (Domain(:,2)-Domain(:,1))/2;
    end
    resMag = vecnorm(resVec,2,1); %length of vector resPos
    resDir = resVec./resMag; resDir(isnan(resDir)) = (1/size(resDir
   ,1))*1./eVec(isnan(resDir)); %unit direction vector of resVec

    radiusCond = resMag<=roi ; %within cone radius, including itself
    cosQA = transpose(resDir'*eVec(:,i)); %dot product of two
   vectors = cos(angle between vectors)
    queryAngle = acos(cosQA); %gives angle in range [0,pi/2]
    angleCond = queryAngle <= phi; %within sensing angle

    isNeighbour = and(radiusCond,angleCond);
    allisNeighbour(i,:) = isNeighbour;
end

if mode == "Visual"
    adjacency = allisNeighbour;
end
if mode == "Auditory"
    adjacency = transpose(allisNeighbour);
end
if mode == "AudioVisual"
    adjacency = or(allisNeighbour,transpose(allisNeighbour));
end

end

```

```
function [pos,eVec] = determineNewParams(adjacency,pos,eVec,v0,eta,
    Domain,typeBC,dt)
% determine new headings and velocity
% input: time k-1
% output: time k

N = size(pos,2);

% Noise
u = 2*(rand(1,N)-0.5); % u=cos(zeta) random in [-1,1]
teta = 2*pi*rand(1,N);
x = sqrt(1-u.^2).*cos(teta);
y = sqrt(1-u.^2).*sin(teta);
z = u;
noise = eta*[x;y;z];

eVec = transpose(adjacency*eVec');
dist = vecnorm(eVec,2,1);
eVec = eVec./dist;

eVec = eVec + noise; % adding noise
dist = vecnorm(eVec,2,1);
eVec = eVec./dist;

pos = pos + v0*eVec*dt; %put this back above to match original
    vicsek
if typeBC == "Periodic"
    pos = mod(pos + (Domain(:,1)-Domain(:,2))/2, (Domain(:,1)-Domain
    (:,2))) - (Domain(:,1)-Domain(:,2))/2;
end
end
```

Listing A.1: Script to execute simulation of 3D Vicsek Model with sensing modes

```
close all
clear
clc

%%
% Compute Polarisations and Cohesions for a range of eta (noise) and
    phi (sensing angle / half-openingAngle)

xL = -5;
yL = xL;
zL = xL;
xU = 5; %length of Domain [distance unit]
yU = xU; %height of Domain [distance unit]
zU = xU; %width of Domain [distance unit]

Domain = [xL xU; yL yU; zL zU];
typeBC = "Periodic";
executePlot = true;

v0 = 0.03; %initial velocity [distance/time]

roi = 1;

rho = 10; %particle density [#/vol]
simTime = 2000; %simulation time [time units]
timeOffset = 1000; %timestep offset for computation of mean
   Polarisation and mean Cohesion
dt = 1; %time step in [time units]

mode1 = 'Auditory';
mode2 = 'Visual';
mode3 = 'AudioVisual';
modes = {mode1,mode2,mode3};

N = floor(rho*det(diag(Domain*[-1;1])));  %number of particles in
   Domain based on density and Domain size [#]
```

```
34
35 %% Initialise all Particles with random positions and orientations
36
37 xInit = (Domain(1,2)-Domain(1,1))*(rand(1,N)+Domain(1,1)/(Domain
       (1,2)-Domain(1,1)));
38 yInit = (Domain(2,2)-Domain(2,1))*(rand(1,N)+Domain(2,1)/(Domain
       (2,2)-Domain(2,1)));
39 zInit = (Domain(3,2)-Domain(3,1))*(rand(1,N)+Domain(3,1)/(Domain
       (3,2)-Domain(3,1)));
40 initialPosition = [xInit;yInit;zInit];
41
42 thetaInit = unifrnd(-pi,pi,1,N);
43 zetaInit = unifrnd(-pi,pi,1,N);
44 initialOrientationAngles = [thetaInit;zetaInit];
45
46 etaRange = [0:0.1:1]; %noise factor
47 phiRange = [0:pi/15:pi]; %sensing half-angle of particle - between 0
       and pi [radians]
48
49 %% Execute Simulation || Compute Polarisation and Cohesion
50
51 path = "rho_"+string(rho)+"t_"+string(simTime);
52 if ~exist(path,'dir')
53     mkdir(path);
54 end
55
56 MN = length(modes);
57 EN = length(etaRange);
58 PN = length(phiRange);
59
60 tStart = tic;
61 for m = 1:length(modes)
62     mode = modes{m};
63     for e = 1:length(etaRange)
64         fprintf("\nRunning Simulation...\n");
65         fprintf('\t Mode: %d of %d\n', m,MN);
```

```
66          fprintf('\t\t eta iter: %d of %d\n',e,EN);
67
68          eta = etaRange(e);
69          parfor p = 1:length(phiRange)
70              phi = phiRange(p);
71              [pos,eVec,DD] = vicsek3d_rajuOpt(N,simTime,dt,roi,phi,
    eta,v0,initialPosition,initialOrientationAngles,Domain,typeBC,
    mode);
72              [pol,coh] = computePolCoh(pos,eVec,roi,simTime,
    timeOffset);
73              cz = computeCZ(DD);
74              parsave3D(path,pos,eVec,DD,pol,coh,cz,eta,phi,mode);
75          end
76      end
77  end
78  tEnd = toc(tStart);
79  fprintf("\nSimulation Complete\n\n");
80  disp("Elapsed Time to Compute Data is "+sprintf('%.4f',tEnd)+"
    seconds");
```

Listing A.2: Script to compute group parameters for 3D Vicsek simulation

```
function [pol,coh] = computePolCoh(posAll,eVecAll,roi,simTime,
    timeOffset)

N = size(posAll,2);
Polarisation = zeros(simTime,1);
Cohesion = zeros(simTime,1);

la = 4*roi;
for k=1:simTime
    Polarisation(k,:) = vecnorm(sum(eVecAll(:,:,k),2),2,1)/N;

    centerOfMass = sum(posAll(:,:,k),2)/N;
    relativePosition = posAll(:,:,k)-centerOfMass;
    Cohesion(k,:) = sum(exp(-vecnorm(relativePosition,2,1)/la))/N;
end
meanPolarisation = mean(Polarisation(1+timeOffset:end,:));
meanCohesion = mean(Cohesion(1+timeOffset:end,:));

pol = struct('all',Polarisation,'mean',meanPolarisation);
coh = struct('all',Cohesion,'mean',meanCohesion);

end
```

Listing A.3: Computation of Polarization and Cohesion

```
function [CZ] = computeCZ(adjacencyAll)
% compute mean largest cluster size
simTime = length(adjacencyAll);
largestClusterSize = zeros(simTime,1);
clusterSizes = cell(simTime,1);
for k = 1:simTime
    g = digraph(adjacencyAll{k});
    weak_bins = conncomp(g,'Type','weak');
    [cz,~] = histcounts(weak_bins,unique(weak_bins));
    clusterSizes{k}=cz;
    largestClusterSize(k,:) = max(cz);
end
meanLargestClusterSize = mean(largestClusterSize);

CZ.all = largestClusterSize;
CZ.mean = meanLargestClusterSize;
end
```

Listing A.4: Computation of Cluster Size

```
function [initialPosition,initialOrientationAngles] =
    generateInitialConditions(Domain,N)
% generate initial positions and headings in 3D domain

xInit = (Domain(1,2)-Domain(1,1))*(rand(1,N)+Domain(1,1)/(Domain
    (1,2)-Domain(1,1)));
yInit = (Domain(2,2)-Domain(2,1))*(rand(1,N)+Domain(2,1)/(Domain
    (2,2)-Domain(2,1)));
zInit = (Domain(3,2)-Domain(3,1))*(rand(1,N)+Domain(3,1)/(Domain
    (3,2)-Domain(3,1)));
initialPosition = [xInit;yInit;zInit];

thetaInit = unifrnd(-pi,pi,1,N);
zetaInit = unifrnd(-pi,pi,1,N);
initialOrientationAngles = [thetaInit;zetaInit];
end
```

Listing A.5: Generate Initial Conditions

```
close all
clear
clc

% Compute Polarisations and Cohesions for a range of eta (noise) and
    phi (sensing angle / half-openingAngle)

xL = -2.5;
yL = xL;
zL = xL;
xU = 2.5; %length of Domain [distance unit]
yU = xU; %height of Domain [distance unit]
zU = xU; %width of Domain [distance unit]

Domain = [xL xU; yL yU; zL zU];
typeBC = "Periodic";
executePlot = true;

v0 = 0.03; %initial velocity [distance/time]
roi = 1;

rho = 10; %particle density [#/vol]
simTime = 2000; %simulation time [time units]
timeOffset = floor(0.5*simTime); %timestep offset for computation of
    mean Polarisation and mean Cohesion
dt = 1; %time step in [time units]

mode1 = "Auditory";
mode2 = "Visual";
mode3 = "AudioVisual";
modes = {mode1,mode2,mode3};

N = floor(rho*det(diag(Domain*[-1;1])));  %number of particles in
   Domain based on density and Domain size [#]

nsims = 20;
```

```
epPair = [ [0.1;2*pi/15], [0.3;5*pi/15],  [0.6;1*pi/15],  [0.8;4*pi
    /15] , [0.3;2*pi/15], [0.5;3*pi/15], [0.7;5*pi/15]];
npairs = size(epPair,2);
nmodes = length(modes);

%% Initialise all Particles with random positions and orientations

xInit = (Domain(1,2)-Domain(1,1))*(rand(1,N)+Domain(1,1)/(Domain
    (1,2)-Domain(1,1)));
yInit = (Domain(2,2)-Domain(2,1))*(rand(1,N)+Domain(2,1)/(Domain
    (2,2)-Domain(2,1)));
zInit = (Domain(3,2)-Domain(3,1))*(rand(1,N)+Domain(3,1)/(Domain
    (3,2)-Domain(3,1)));
initialPosition = [xInit;yInit;zInit];

thetaInit = unifrnd(-pi,pi,1,N);
zetaInit = unifrnd(-pi,pi,1,N);
initialOrientationAngles = [thetaInit;zetaInit];

%% Execute Simulation || Compute Polarisation and Cohesion

path = "rho_"+string(rho)+"t_"+string(simTime);
if ~exist(path,'dir')
    mkdir(path);
end

offset1 = 0;
offset2 = 3;
tStart = tic;

for pairk = (1+offset1):(npairs-offset2)
    epVals = epPair;
    eta = epVals(1,pairk);
    phi = epVals(2,pairk);

    POL = cell(nmodes,nsims);
```

```
66      COH = cell(nmodes,nsims);
67      CZ = cell(nmodes,nsims);
68
69      polTime = cell(nmodes,nsims);
70      polTimeMean = zeros(nmodes,simTime);
71      cohTime = cell(nmodes,nsims);
72      cohTimeMean = zeros(nmodes,simTime);
73      czTime = cell(nmodes,nsims);
74      czTimeMean = zeros(nmodes,simTime);
75
76      for simk = 1:nsims
77          fprintf("\nRunning Simulation...\n");
78          fprintf('\t pair: %d of %d\n',pairk,npairs);
79          fprintf('\t sim: %d of %d\n', simk,nsims);
80
81          parfor modek = 1:nmodes
82              mode = modes{modek};
83              fprintf('\t\t mode: %d of %d\n', modek,nmodes);
84
85              [initialPosition,initialOrientationAngles] =
    generateInitialConditions(Domain,N);
86              [pos,eVec,DD] = vicsek3d(N,simTime,dt,roi,phi,eta,v0,
    initialPosition,initialOrientationAngles,Domain,typeBC,mode);
87
88              [POL{modek,simk},COH{modek,simk}] = computePolCoh(pos,
    eVec,roi,simTime,timeOffset);
89              CZ{modek,simk} = computeCZ(DD);
90
91              polTime{modek,simk} = POL{modek,simk}.all;
92              polTimeMean(modek,:) = polTimeMean(modek,:) + (POL{modek
    ,simk}.all.')/nsims;
93
94              cohTime{modek,simk} = COH{modek,simk}.all;
95              cohTimeMean(modek,:) = cohTimeMean(modek,:) + (COH{modek
    ,simk}.all.')/nsims;
96
```

```
97              czTime{modek,simk} = CZ{modek,simk}.all;
98              czTimeMean(modek,:) = czTimeMean(modek,:) + (CZ{modek,
    simk}.all.')/nsims;
99
100         end
101     end
102     clear pos eVec DD
103     save(path+"/data_pair"+string(pairk)+".mat","POL","COH","CZ","
    polTime","polTimeMean","cohTime","cohTimeMean","czTime","
    czTimeMean","epVals","epPair","pairk","Domain","N","rho","eta","
    phi","simTime","timeOffset","modes",'-v7.3');
104 end
105 tEnd = toc(tStart);
106 fprintf("\nSimulation Complete\n\n");
107 disp("Elapsed Time to Compute Data is "+sprintf('%.4f',tEnd)+"
    seconds");
108 clear POL COH polTime cohTime polTimeMean cohTimeMean czTime
    czTimeMean pairk modek simk
```

Listing A.6: Script to execute Monte-Carlo Simulation

A.2 Offset Vicsek model

```
function [posAll,eVecAll,thetaAll,DD,Neighbours] = vicsek2d(N,
    simTime,dt,roi,phi,sensingOffset,eta,v0,initialPosition,
    initialOrientation,domain,typeBC,mode)

%Initialise all Particles with random positions, orientations, and
    initial velocity within the grid
pos = initialPosition;
theta = initialOrientation; % theta = unifrnd(-pi,pi,1,N);
eVec = [cos(theta);sin(theta)]; %heading of particle

%Simulation
DD = cell(simTime,1);
thetaAll = zeros(simTime,N);
posAll = zeros(2,N,simTime);
eVecAll = zeros(2,N,simTime);
Neighbours = cell(N,simTime);
for k = 1:dt:simTime
    posAll(:,:,k) = pos;
    thetaAll(k,:) = theta;
    eVecAll(:,:,k) = eVec;

    [D,allNeighboursIDX] = determineNeighbours(mode,typeBC,pos,theta
    ,roi,phi,sensingOffset,domain);
    DD{k} = D;
    Neighbours(:,k) = allNeighboursIDX;

    [pos,eVec,theta] =  determineNewParams(typeBC,allNeighboursIDX,
    pos,v0,eta,theta,dt,domain);
end
end


function [adjacency,allNeighboursIDX] = determineNeighbours(mode,
    typeBC,pos,theta,roi,phi,sensingOffset,domain)
```

```
% for each particle, if a surrounding particle is within sensing
% region, then that particle is considered a neighbour
N = length(theta);
allisNeighbour = zeros(N);
allNeighboursIDX = cell(N,1);
eVec = [cos(theta+sensingOffset);sin(theta+sensingOffset)];

for i=1:N
    resVec = pos-pos(:,i); %vectors from ith particle to all other
    particles
    if typeBC == "Periodic"
        resVec = mod(resVec+(domain(:,2)-domain(:,1) )/2, domain
    (:,2)-domain(:,1) ) - (domain(:,2)-domain(:,1))/2;
    end
    resMag = vecnorm(resVec,2,1); %length of vector resPos
    resDir = resVec./resMag; resDir(isnan(resDir)) = (1/size(reVec
    ,1))*1./eVec(isnan(resDir)); %unit direction vector of resVec
    radiusCond = resMag<=roi ; %within cone radius, including itself

    dp = transpose(resDir'*eVec(:,i)); %dot product of two vectors =
    cos(angle between vectors)
    queryAngle = acos(dp); %gives angle in range [0,pi/2]
    angleCond = cos(queryAngle)-cos(phi) > -0.00000000000001;

    isNeighbour = and(radiusCond,angleCond);
    allisNeighbour(i,:) = isNeighbour;
end

if mode == "Visual"
    VisualNeighbourMat = allisNeighbour;
    adjacency = VisualNeighbourMat;
end
if mode == "Auditory"
    AudioNeighbourMat = transpose(allisNeighbour);
    adjacency = AudioNeighbourMat;
end
```

```
if mode == "AudioVisual"
    VisualNeighbourMat = allisNeighbour;
    AudioNeighbourMat = transpose(allisNeighbour);
    AudioVisualNeighbourMat = VisualNeighbourMat | AudioNeighbourMat;
    adjacency = AudioVisualNeighbourMat;
end
for i = 1:N
    allNeighboursIDX{i} = find(adjacency(i,:));
end
end


function [pos,eVec,ttheta] = determineNewParams(typeBC,allNeighboursIDX,pos,v0,eta,theta,dt,domain)
% determine new orientation, velocity, and positions
N = length(theta);
thetaAvg = zeros(size(theta));
deltaTheta = unifrnd(-eta/2,eta/2,1,N); %random number chosen with uniform probability on interval [-eta/2,eta/2]

for i=1:N
    thetaAvg(i) = atan2(sum(sin(theta(allNeighboursIDX{i}))),sum(cos(theta(allNeighboursIDX{i}))));
end
ttheta = thetaAvg + deltaTheta; %new direction or orientation with respect to origin of cartesian

pos = pos+ v0*[cos(theta);sin(theta)]*dt;
if typeBC == "Periodic"
    pos = mod(pos + (domain(:,2)-domain(:,1))/2, domain(:,2)-domain(:,1)) - (domain(:,2)-domain(:,1))/2;
end
eVec = [cos(ttheta);sin(ttheta)]; %new heading direction vector
end
```

Listing A.7: Script to execute simulation of 2D Vicsek Model with offset sensing

```
function [pol,coh,cz,am] = computeGroupParameters(posAll,eVecAll,
    adjacencyAll,roi,simTime,timeOffset)
% compute polarisation, cohesion, cluster size, angular momentum
N = size(posAll,2);
Polarisation = zeros(simTime,1);
Cohesion = zeros(simTime,1);
largestClusterSize = zeros(simTime,1);
clusterSizes = cell(simTime,1);
AngularMomentum = zeros(simTime,1);

la = 4*roi;

for k=1:simTime
    pos = posAll(:,:,k);
    vDir = eVecAll(:,:,k);
    DD = adjacencyAll{k};
    centerOfMass = sum(pos,2)/N;
    relativePosition = pos-centerOfMass;

    Polarisation(k,:) = vecnorm(sum(vDir,2),2,1)/N;
    Cohesion(k,:) = sum(exp(-vecnorm(relativePosition,2,1)/la))/N;

    g = digraph(DD);
    weak_bins = conncomp(g,'Type','weak');
    [clusterSizes{k,:},~] = histcounts(weak_bins,unique(weak_bins));
    largestClusterSize(k,:) = max(clusterSizes{k,:});
    crossProd = cross([relativePosition;zeros(1,N)],[vDir;zeros(1,N)
    ]);
    AngularMomentum(k,:) = vecnorm(sum(crossProd,2),2,1) / sum(
    vecnorm(relativePosition,2,1).*vecnorm(vDir,2,1));
end
meanPolarisation = mean(Polarisation(1+timeOffset:end,:));
meanCohesion = mean(Cohesion(1+timeOffset:end,:));
meanLargestClusterSize = mean(largestClusterSize);
meanAngularMomentum = mean(AngularMomentum);

```

```
pol = struct('all',Polarisation,'mean',meanPolarisation);
coh = struct('all',Cohesion,'mean',meanCohesion);
cz = struct('all',clusterSizes,'largestSizes',largestClusterSize,'
    meanLargest',meanLargestClusterSize);
am = struct('all',AngularMomentum,'mean',meanAngularMomentum);
end
```

Listing A.8: Computation of Polarization Cohesion and Cluster Size

```
close all
clear
clc

rho = 5;
simTime = 5000;
offset = 3000;
L = 10;

b = 100;
bh = 10;
bv = b/bh;

binLength = L/bh;
binHeight = L/bv;

sensingOffsetRange = [0:pi/6:2*pi];
etaRange = [0.1:0.1:0.9];
phiRange = [0:pi/15:pi];

numSensingOffsets = length(sensingOffsetRange);

numEta = length(etaRange);
numPhi = length(phiRange);

b0 = zeros(numEta,numPhi,simTime-offset);
coverage = zeros(numEta,numPhi);

```

```
path = "rho_"+string(rho)+"t_"+string(simTime);

%%

for s = 1:numSensingOffsets
    % clc;
    % fprintf('Sensing Range: %d degrees  |  %d of %d\n', rad2deg(
    sensingOffsetRange(s)), s, numSensingOffsets);
    sensingOffset = sensingOffsetRange(s);
    for ek = 1:numEta
        eta = etaRange(ek);
        % fprintf('\t eta: %.1f  | %d of %d\n',etaRange(ek),ek,
    numEta);
        for pk = 1:numPhi
            phi = phiRange(pk);
            pths = path+"/offset_"+string(rad2deg(sensingOffset))+"/
    phi_"+string(rad2deg(phi))+"/eta_"+string(eta);
            load(pths+"/TrajectoryData.mat");
            for tt = 1+offset:simTime
                [hasAgent,numAgents] = hasAgentHist(bh,bv,binLength,
    binHeight,pos(:,:,tt));
                b0(ek,pk,tt-offset) = sum(double(hasAgent),'all');
            end
            coverage(ek,pk,s) = mean(squeeze(b0(ek,pk,:))/b);
        end
    end
end
function [hasAgent,numAgents] = hasAgentHist(bh,bv,binLength,
    binHeight,pos)
numAgents = histcounts2(pos(1,:),pos(2,:),'NumBins',[bh,bv],'
    BinWidth',[binHeight,binLength]);
hasAgent = numAgents>0;
end
```

Listing A.9: Computation of coverage

```
close all
clear
clc

% Compute Polarisations, Cohesions, Angular Momemtum, and Cluster Size for a range of eta (noise) and phi (sensing angle / half-openingAngle)
% Visual Sensing Mode for a range of sensing offsets

typeBC = "Periodic";% BC: Periodic, none

L0 = -5;
H0 = L0;
L1 = 5; %length of domain [distance unit]
H1 = L1; %height of domain [distance unit]
domain = [L0,L1;H0,H1];

v0 = 0.03; %initial velocity [distance/time]
roi = 1;

rho = 5; %particle density [#/area]
N = floor(rho*det(diag(domain*[-1;1]))); %number of particles in domain based on density and domain size [#]

%% Initialise all Particles with random positions and orientations
xInit = (domain(1,2)-domain(1,1))*(rand(1,N)+domain(1,1)/(domain(1,2)-domain(1,1)));
yInit = (domain(2,2)-domain(2,1))*(rand(1,N)+domain(2,1)/(domain(2,2)-domain(2,1)));
thetaInit = unifrnd(-pi,pi,1,N);
initialPosition = [xInit;yInit];
initialOrientation = thetaInit;

%% Execute Simulation || Compute Polarisation and Cohesion
% Preambles

```

```
etaRange = [0:0.1:5]; %noise factor
phiRange = [0:pi/15:pi]; %sensing half-angle of particle - between 0
    and pi [radians]
sensingOffsetRange = [0,pi]; %sensing region offset


dt = 1; %time step in [time units]
simTime = 5000; %simulation time [time units]
timeOffset = 1000; %timestep offset for computation of mean
   Polarisation and mean Cohesion

path = "rho_"+string(rho)+"t_"+string(simTime)+"_new2";
mkdir(path);

mode1 = 'Visual';
modes = {mode1};

MeanPolarisations = cell(length(modes),length(sensingOffsetRange));
MeanCohesions = cell(length(modes),length(sensingOffsetRange));
MeanLargestClusterSizes = cell(length(modes),length(
   sensingOffsetRange));
MeanAngularMomentums = cell(length(modes),length(sensingOffsetRange)
   );

AllPolarisations = cell(length(modes),length(sensingOffsetRange));
AllCohesions = cell(length(modes),length(sensingOffsetRange));
AllAngularMomentums = cell(length(modes),length(sensingOffsetRange))
   ;

tStart = tic;
for m = 1:length(modes)
    mode = modes{m};
    for s = 1:length(sensingOffsetRange)
        MeanPolarisations{m,s} = zeros(length(etaRange),length(
   phiRange));
        MeanCohesions{m,s} = zeros(length(etaRange),length(phiRange)
```

```
);
62      MeanLargestClusterSizes{m,s} = zeros(length(etaRange),length
(phiRange));
63      MeanAngularMomentums{m,s} = zeros(length(etaRange),length(
phiRange));
64
65      AllPolarisations{m,s} =  cell(length(etaRange),length(
phiRange));
66      AllCohesions{m,s} =  cell(length(etaRange),length(phiRange))
;
67      AllAngularMomentums{m,s} = cell(length(etaRange),length(
phiRange));
68
69      sensingOffset = sensingOffsetRange(s);
70      for e = 1:length(etaRange)
71          eta = etaRange(e);
72          for p = 1:length(phiRange)
73              phi = phiRange(p);
74              [pos,eVec,~,DD] = vicsek2d(N,simTime,dt,roi,phi,
sensingOffset,eta,v0,initialPosition,initialOrientation,domain,
typeBC,mode);
75              [pol,coh,cz,am] = computeGroupParameters(pos,eVec,DD
,roi,simTime,timeOffset);
76              MeanPolarisations{m,s}(e,p) = pol.mean;
77              MeanCohesions{m,s}(e,p) = coh.mean;
78              MeanLargestClusterSizes{m,s}(e,p) = cz.meanLargest;
79              MeanAngularMomentums{m,s}(e,p) = am.mean;
80              AllPolarisations{m,s}{e,p} = pol.all;
81              AllCohesions{m,s}{e,p} = coh.all;
82              AllAngularMomentums{m,s}{e,p} = am.all;
83
84              %save data for simulation
85              pths = path+"/offset_"+string(rad2deg(sensingOffset)
+"/phi_"+string(rad2deg(phi))+"/eta_"+string(eta));
86              mkdir(pths);
87              save(pths+"/TrajectoryData.mat","pos","eVec","DD",'-
```

```
    v7.3');
88                  % clear unnecessary data
89                  clear pos eVec DD pol coh cz am pths
90              end
91          end
92      end
93  end
94  tEnd = toc(tStart);
95  save(path+"/data.mat");
96  disp("Elapsed Time is "+sprintf('%.7f',tEnd)+" seconds");
```

Listing A.10: Extended parameter analysis for Flipped Sensing

```
close all
clear
clc


% Comparison of flipped and unflipped sensing

%% Preambles
typeBC = "none";% BC: Periodic, none
mode = "Visual";

L0 = -20;
H0 = L0;
L1 = 20; %upper x bound of domain [distance unit]
H1 = L1; %upper y bound of domain [distance unit]
domain = [L0,L1;H0,H1];

v0 = 0.03; %initial velocity [distance/time]
roi = 1;
% phi = 3*pi/15;
eta = 0;

simTime = 1000;
dt = 1;


%% Variables
strat = 60;
theta1Range = 0:pi/strat:pi;
phiRange = pi/15:pi/15:pi;
diffClosestApproach = zeros(length(theta1Range),length(phiRange));

sensingOffset1 = 0;
sensingOffset2 = pi;
sensingOffsetModes = [0,pi];
numAgents = 2;
```

```
37
38 for t = 1:length(theta1Range)
39     for p = 1:length(phiRange)
40
41         phi = phiRange(p);
42
43         leadStartPos = [0;-2.25];
44         leaderDir = pi/2;
45         followerDir = theta1Range(t);
46         followerPos = [5;0];
47
48         P1init = [leadStartPos,followerPos];
49         T1init = [leaderDir,followerDir];
50         N1 = length(T1init);
51
52         P2init = [leadStartPos,followerPos];
53         T2init = [leaderDir,followerDir];
54         N2 = length(T2init);
55
56         Pinit = cat(3,P1init,P2init); %concatenate in 3rd dimension.
     coordinate x numAgents x numModes
57         Tinit = [T1init;T2init];
58
59         % 1 and 2 in P1init. P2init, T1init, T2init indicate modes (
    unflipped and flipped)
60
61         pos = cell(1,length(sensingOffsetModes));
62         eVec = cell(1,length(sensingOffsetModes));
63         resVec = cell(1,length(sensingOffsetModes));
64         dist = cell(1,length(sensingOffsetModes));
65         closestDist = zeros(1,length(sensingOffsetModes));
66
67         for s = 1:length(sensingOffsetModes)
68             [pp,eV] = vicsek2d(numAgents,simTime,dt,roi,phi,
    sensingOffsetModes(s),eta,v0,Pinit(:,:,s),Tinit(s,:),domain,
    typeBC,mode);
```

```
            pos{s} = pp; eVec{s} = eV;
            resVec{s} = squeeze(pp(:,1,:)-pp(:,2,:));
            if typeBC == "Periodic"
                resVec{s} = mod(resVec{s}+(domain(:,2)-domain(:,1))
    /2,domain(:,2)-domain(:,1))-(domain(:,2)-domain(:,1))/2;
            end
            dist{s} = vecnorm(resVec{s},2,1); dd = dist{s};
            closestDist(s) = abs(min(dd(abs(dd)>0)));
        end
        distDiff = closestDist(2) - closestDist(1); %differerence
    between two modes: flipped-regular
        diffClosestApproach(t,p) = (distDiff);
     end
end
save('data'+string(strat)+'.mat');
```

Listing A.11: Closest approach analysis for Flipped Sensing

Bibliography

[1] Tamás Vicsek and Anna Zafeiris. Collective motion. *Physics Reports*, 517(3):71–140, 2012. Collective motion.

[2] Tamas Vicsek, Andras Czirok, Eshel Ben-Jacob, Inon Cohen, and Ofer Shochet. Novel type of phase transition in a system of self-driven particles. *Physical Review Letters*, 75:1226–1229, Aug 1995.

[3] Subhradeep Roy, Masoud Jahromi Shirazi, Benjamin Jantzen, and Nicole Abaid. Effect of visual and auditory sensing cues on collective behavior in vicsek models. *Physical Review E*, 100(6):062415, Dec 2019.

[4] Junqiao Zhang, Qiang Qu, and Xue-Bo Chen. A review on collective behavior modeling and simulation: building a link between cognitive psychology and physical action. *Applied Intelligence*, 53(21):25954–25983, 2023.

[5] Moumita Das, Christoph F. Schmidt, and Michael Murrell. Introduction to active matter. *Soft Matter*, 16:7185–7190, 2020.

[6] Irene Giardina. Collective behavior in animal groups: theoretical models and empirical studies. *HFSP journal*, 2:205–19, Aug 2008.

[7] Alessandro Attanasi, Andrea Cavagna, Lorenzo Castello, Irene Giardina, Stefania Melillo, Leonardo Parisi, Oliver Pohl, Bruno Rossaro, Edward Shen, Edmondo Silvestri, and Massimiliano Viale. Collective behaviour without collective order in wild swarms of midges. *PLoS computational biology*, 10:e1003697, 07 2014.

[8] Benno Liebchen and Demian Levis. Collective behavior of chiral active matter: Pattern formation and enhanced flocking. *Phys. Rev. Lett.*, 119:058002, Aug 2017.

[9] Samuel R. McCandlish, Aparna Baskaran, and Michael F. Hagan. Spontaneous segregation of self-propelled particles with different motilities. *Soft Matter*, 8:2527–2534, 2012.

[10] András Czirók, Eshel Ben-Jacob, Inon Cohen, and Tamás Vicsek. Formation of complex bacterial colonies via self-generated vortices. *Phys. Rev. E*, 54:1791–1801, Aug 1996.

[11] Habiba Drias, Lydia Sonia Bendimerad, and Yassine Drias. A three-phase artificial orcas algorithm for continuous and discrete problems. *International Journal of Applied Metaheuristic Computing (IJAMC)*, 13(1):1–20, 2022.

[12] Brian L. Partridge. The structure and function of fish schools. *Scientific American*, 246 6:114–23, 1982.

[13] Evelyn Shaw. Schooling Fishes. *American Scientist*, 66(2):166–175, March 1978.

[14] Iain D. Couzin, Jens Krause, Nigel R. Franks, and Simon A. Levin. Effective leadership and decision-making in animal groups on the move. *Nature*, 433(7025):513–516, 2005.

[15] R. Eftimie, G. de Vries, and M. A. Lewis. Complex spatial group patterns result from different animal communication mechanisms. *Proceedings of the National Academy of Sciences*, 104(17):6974–6979, 2007.

[16] Ronald Nowak, Larry Watkins, and L. Mech. The wolf: The ecology and behavior of an endangered species. *Journal of Mammalogy*, 52:644, 08 1971.

[17] Craig W. Reynolds. Flocks, herds and schools: A distributed behavioral model. *SIGGRAPH Comput. Graph.*, 21(4):25–34, aug 1987.

[18] Tom Wenseleers. The superorganism: The beauty, elegance, and strangeness of insect societies . by bert hölldobler and e. o. wilson. *Quarterly Review of Biology - QUART REV BIOL*, 85:114–115, 03 2010.

[19] Deborah M. Gordon. The organization of work in social insect colonies. *Nature*, 380(6570):121–124, 1996.

[20] Caroline H. Brighton, Adrian L. R. Thomas, and Graham K. Taylor. Terminal attack trajectories of peregrine falcons are described by the proportional navigation guidance law of missiles. *Proceedings of the National Academy of Sciences*, 114(51):13495–13500, 2017.

[21] David Jachowski. The amboseli elephants: A long-term perspective on a long-lived mammal by c. j. moss; h. croze; p. c. lee. *Journal of Mammalogy*, 93:294–295, 02 2012.

[22] Guillaume J Dury, Jacqueline C. Bede, and Donald M Windsor. Preemptive circular defence of immature insects: Definition and occurrences of cycloalexy revisited. *Psyche*, 2014:1–13, 2014.

[23] L. Giomi, L. Mahadevan, B. Chakraborty, and M. F. Hagan. Excitable patterns in active nematics. *Phys. Rev. Lett.*, 106:218101, May 2011.

[24] Francesco Ginelli. The physics of the vicsek model. *The European Physical Journal Special Topics*, 225(11):2099–2117, 2016.

[25] Edward O. Wilson. *The insect societies.* Belknap Press: An Imprint of Harvard University Press, 1971.

[26] A. Schadschneider, D. Chowdhury, and K. Nishinari. From ant trails to pedestrian dynamics — learning from nature. In Nathalie Waldau, Peter Gattermann, Hermann Knoflacher, and Michael Schreckenberg, editors, *Pedestrian and Evacuation Dynamics 2005*, pages 481–495, Berlin, Heidelberg, 2007. Springer Berlin Heidelberg.

[27] Leah Edelstein-Keshet. Simple models for trail-following behaviour; trunk trails versus individual foragers. *Journal of Mathematical Biology*, 32:303–328, 1994.

[28] Matthias L. Zorn, Anna-Kristina Marel, Felix J. Segerer, and Joachim O. Rädler. Phenomenological approaches to collective behavior in epithelial cell migration. *Biochimica et Biophysica Acta (BBA) - Molecular Cell Research*, 1853(11, Part B):3143–3152, 2015. Mechanobiology.

[29] Mark K. Transtrum and Peng Qiu. Bridging mechanistic and phenomenological models of complex biological systems. *PLOS Computational Biology*, 12(5):1–34, 05 2016.

[30] Renaud Bastien and Pawel Romanczuk. A model of collective behavior based purely on vision. *Science advances*, 6:eaay0792, Feb 2020.

[31] Alexander Mogilner and Leah Edelstein-Keshet. A non-local model for a swarm. *Journal of mathematical biology*, 38:534–570, 1999.

[32] E. F. Keller and L. A. Segel. Traveling bands of chemotactic bacteria: a theoretical analysis. *Journal of theoretical biology*, 30:235–48, Feb 1971.

[33] Veysel Gazi. On lagrangian dynamics based modeling of swarm behavior. *Physica D: Nonlinear Phenomena*, 260:159–175, 2013. Emergent Behaviour in Multiparticle Systems with Non-local Interactions.

[34] Sudipto Mukherjee, Debdipta Goswami, and Sarthak Chatterjee. A lagrangian approach to modeling and analysis of a crowd dynamics. *IEEE Transactions on Systems, Man, and Cybernetics: Systems*, 45:1–1, 06 2015.

[35] Ichiro Aoki. A simulation study on the schooling mechanism in fish. *Nippon Suisan Gakkaishi*, 48(8):1081–1088, 1982.

[36] Iain D. Couzin, Jens Krause, Richard James, Graeme D. Ruxton, and Nigel R. Franks. Collective memory and spatial sorting in animal groups. *Journal of Theoretical Biology*, 218(1):1–11, 2002.

[37] Pau Clusella and Romualdo Pastor-Satorras. Phase transitions on a class of generalized vicsek-like models of collective motion. *Chaos: An Interdisciplinary Journal of Nonlinear Science*, 31(4):043116, 04 2021.

[38] Subhradeep Roy, Kayla Howes, Rolf Muller, Sachit Butail, and Nicole Abaid. Extracting interactions between flying bat pairs using model-free methods. *Entropy*, 21(1):42, 2019.

[39] U. Kadri, F. Brümmer, and A. Kadri. Random patterns in fish schooling enhance alertness: A hydrodynamic perspective. *Europhysics Letters*, 116(3):34002, dec 2016.

[40] Xinbiao Lu, Chi Zhang, Chen Huang, and Buzhi Qin. Research on swarm consistent performance of improved vicsek model with neighbors degree. *Physica A: Statistical Mechanics and its Applications*, 588:126567, 2022.

[41] Hongli Hu, Fuquan Zhu, Liping Yang, and Weiyi Ren. Design of swarm control based on vicsek model. In Sandeep Saxena and Cairong Zhao, editors, *International Conference on Algorithms, High Performance Computing, and Artificial Intelligence (AHPCAI 2023)*, volume 12941, page 129414Z. International Society for Optics and Photonics, SPIE, 2023.

[42] Alexandre Morin, Jean-Baptiste Caussin, Christophe Eloy, and Denis Bartolo. Collective motion with anticipation flocking, spinning, and swarming. *Phys. Rev. E*, 91:012134, Jan 2015.

[43] Xiaocheng Wang, Hui Zhao, and Li Li. An improved vicsek model of swarms based on a new neighbor strategy considering view and distance. *Applied Sciences*, 13(20), 2023.

[44] Xin-Guang Wang, Chen-Ping Zhu, Chuan-Yang Yin, Dong-Sheng Hu, and Zhi-Jun Yan. A modified vicsek model for self-propelled agents with exponential neighbor weight and restricted visual field. *Physica A: Statistical Mechanics and its Applications*, 392(10):2398–2405, 2013.

[45] Bao-Mei Tian, Han-Xin Yang, Wei Li, Wen-Xu Wang, Bing-Hong Wang, and Tao Zhou. Optimal view angle in collective dynamics of self-propelled agents. *Phys. Rev. E*, 79:052102, May 2009.

[46] Yu-Jian Li, Su Wang, Zhong-Lin Han, Bao-Mei Tian, Zhen-Dong Xi, and Bing-Hong Wang. Optimal view angle in the three-dimensional self-propelled particle model. *Europhysics Letters*, 93(6):68003, 2011.

[47] Angelo Forli and Michael M. Yartsev. Hippocampal representation during collective spatial behaviour in bats. *Nature*, 621(7980):796–803, 2023.

[48] Gerald Kerth. Causes and consequences of sociality in bats. *BioScience*, 58(8):737–746, 09 2008.

[49] Angeles Salles, Clarice Anna Diebold, and Cynthia F. Moss. Echolocating bats accumulate information from acoustic snapshots to predict auditory object motion. *Proceedings of the National Academy of Sciences of the United States of America*, 117:29229–29238, Nov 2020.

[50] Paloma Carrasco, Francisco Cuesta, Rafael Caballero, Francisco J. Perez-Grau, and Antidio Viguria. Multi-sensor fusion for aerial robots in industrial gnss-denied environments. *Applied Sciences*, 11(9), 2021.

[51] Amjad Yousef Majid, Casper van der Horst, Tomas van Rietbergen, David JohannesZwart, and R Venkatesha Prasad. Lightweight audio source localization for swarm robots. In *2021 IEEE 18th Annual Consumer Communications and Networking Conference (CCNC)*, pages 1–6, 2021.

[52] Linan Zu, Peng Yang, Yan Zhang, Lingling Chen, and Hao Sun. Study on navigation system of mobile robot based on auditory localization. In *2009 IEEE International Conference on Robotics and Biomimetics (ROBIO)*, pages 321–326, 2009.

[53] Michele Ballerini, Nicola Cabibbo, Raphael Candelier, Andrea Cavagna, Evaristo Cisbani, Irene Giardina, Vivien Lecomte, Alberto Orlandi, Giorgio Parisi, and Andrea Procaccini. Interaction ruling animal collective behavior depends on topological rather than metric distance: Evidence from a field study. *Proceedings of the National Academy of Sciences*, 105(4):1232–1237, 2008.

[54] Michele Ballerini, Nicola Cabibbo, Raphael Candelier, Andrea Cavagna, Evaristo Cisbani, Irene Giardina, Alberto Orlandi, Giorgio Parisi, Andrea Procaccini, Massimiliano Viale, et al. Empirical investigation of starling flocks: a benchmark study in collective animal behaviour. *Animal behaviour*, 76(1):201–215, 2008.

[55] Brian L Partridge, Tony Pitcher, J Michael Cullen, and John Wilson. The three-dimensional structure of fish schools. *Behavioral Ecology and Sociobiology*, 6:277–288, 1980.

[56] Iain D. Couzin and Nigel R. Franks. Self-organized lane formation and optimized traffic flow in army ants. *Proceedings of the Royal Society of London. Series B: Biological Sciences*, 270(1511):139–146, 2003.

[57] Julia K. Parrish, Steven V. Viscido, and Daniel Grunbaum. Self-organized fish schools: an examination of emergent properties. *The Biological Bulletin*, 202(3):296–305, 2002.

[58] Nicole Abaid and Maurizio Porfiri. Fish in a ring: spatio-temporal pattern formation in one-dimensional animal groups. *Journal of The Royal Society Interface*, 7(51):1441–1453, 2010.

[59] Sachit Butail, Nicholas C. Manoukis, Moussa Diallo, JosÃfÂfÃ‚Â© M. C. Ribeiro, and Derek A. Paley. The dance of male anopheles gambiae in wild mating swarms. *Journal of Medical Entomology*, 50(3):552–559, 2013.

[60] T. J. Pitcher, A. E. Magurran, and I. J. Winfield. Fish in larger shoals find food faster. *Behavioral Ecology and Sociobiology*, 10(2):149–151, 1982.

[61] Christos C. Ioannou, Vishwesha Guttal, and Iain D. Couzin. Predatory fish select for coordinated collective motion in virtual prey. *Science*, 337(6099):1212–1215, 2012.

[62] D. P. Cowan. Group living in the european rabbit (oryctolagus cuniculus): mutual benefit or resource localization? *The Journal of Animal Ecology*, pages 779–795, 1987.

[63] Chad M. Topaz, Andrea L. Bertozzi, and Mark A. Lewis. A nonlocal continuum model for biological aggregation. *Bulletin of Mathematical Biology*, 68(7):1601, 2006.

[64] Matteo Aureli and Maurizio Porfiri. Coordination of self-propelled particles through external leadership. *Europhysics Letters*, 92(4):40004, 2010.

[65] Alethea BT Barbaro, Kirk Taylor, Peterson F Trethewey, Lamia Youseff, and Bjorn Birnir. Discrete and continuous models of the dynamics of pelagic fish: application to the capelin. *Mathematics and Computers in Simulation*, 79(12):3397–3414, 2009.

[66] Wei Zhang and Yonghui Yang. A survey of mathematical modeling based on flocking system. *Vibroengineering PROCEDIA*, 13:243–248, 2017.

[67] M Aldana, H Larralde, and B Vázquez. On the emergence of collective order in swarming systems: a recent debate. *International Journal of Modern Physics B*, 23(18):3661–3685, 2009.

[68] I Tarras, R Bakir, A Hader, M Mazroui, Dorilson Cambui, and Y Boughaleb. The combined effect of repulsion zone and initial velocity on vicsek model. *Sensor Letters*, 16(2):123–127, 2018.

[69] Hugues Chate, Francesco Ginelli, Guillaume Gregoire, Fernando Peruani, and Franck Raynaud. Modeling collective motion: variations on the vicsek model. *The European Physical Journal B*, 64(3):451–456, 2008.

[70] András Czirók, Mária Vicsek, and Tamás Vicsek. Collective motion of organisms in three dimensions. *Physica A: Statistical Mechanics and its Applications*, 264(1):299–304, 1999.

[71] Mihir Durve and Ahmed Sayeed. First-order phase transition in a model of self-propelled particles with variable angular range of interaction. *Phys. Rev. E*, 93:052115, May 2016.

[72] Jeanette A. Thomas, Cynthia F. Moss, and Marianne Vater. *Echolocation in bats and dolphins*. University of Chicago Press, 2004.

[73] Dan Gorbonos, Reuven Ianconescu, James G. Puckett, Rui Ni, Nicholas T. Ouellette, and Nir S. Gov. Long-range acoustic interactions in insect swarms: an adaptive gravity model. *New Journal of Physics*, 18(7):073042, 2016.

[74] Masoud Jahromi Shirazi and Nicole Abaid. Collective behavior in groups of self-propelled particles with active and passive sensing inspired by animal echolocation. *Physical Review E*, 98(4):042404, 2018.

[75] Yossi Yovel and Stefan Greif. Bats-using sound to reveal cognition. *Field and Laboratory Methods in Animal Cognition: A Comparative Guide*, pages 31–59, 2018.

[76] Zhaodan Kong, Nathan Fuller, Shuai Wang, Kayhan Ozcimder, Erin Gillam, Diane Theriault, Margrit Betke, and John Baillieul. Perceptual modalities guiding bat flight in a native habitat. *Scientific Reports*, 6:27252, 2016.

[77] Rebecca E. Whiley and Rachel M. Day. Multisensory integration of echolocation and vision in mammals. *Western Undergraduate Psychology Journal*, 7(1), 2019.

[78] Barry E. Stein and Terrence R. Stanford. Multisensory integration: current issues from the perspective of the single neuron. *Nature reviews neuroscience*, 9(4):255–266, 2008.

[79] Dara N. Orbach and Brock Fenton. Vision impairs the abilities of bats to avoid colliding with stationary obstacles. *PLoS One*, 5(11), 2010.

[80] Johan Eklof, A. Monica Svensson, and Jens Rydell. Northern bats, *eptesicus nilssonii*, use vision but not flutter?detection when searching for prey in clutter. *Oikos*, 99(2):347–351, 2002.

[81] Jens Rydell and Johan Eklof. Vision complements echolocation in an aerial-hawking bat. *Naturwissenschaften*, 90(10):481–483, 2003.

[82] Arjan Boonman, Yinon Bar-On, and Yossi Yovel. It's not black or white - on the range of vision and echolocation in echolocating bats. *Frontiers in physiology*, 4:248, 2013.

[83] Sasha Danilovich, Anand Krishnan, Wu-Jung Lee, Ivailo Borrisov, Ofri Eitan, Gabor Kosa, Cynthia F. Moss, and Yossi Yovel. Bats regulate biosonar based on the availability of visual information. *Current Biology*, 25(23):R1124–R1125, 2015.

[84] Subhradeep Roy and Nicole Abaid. Consensus of conspecific agents via collaborative and antagonistic interactions. In *Dynamic Systems and Control Conference*, volume 57267, page V003T37A004. American Society of Mechanical Engineers, 2015.

[85] Subhradeep Roy and Nicole Abaid. On the effect of collaborative and antagonistic interactions on synchronization and consensus in networks of conspecific agents. *IEEE Transactions on Automatic Control*, 61(12):4063–4068, 2016.

[86] Subhradeep Roy and Jeremy Lemus. How does the fusion of sensory information from audition and vision impact collective behavior? *Frontiers in Applied Mathematics and Statistics*, 7:758711, 2021.

[87] William Bialek, Andrea Cavagna, Irene Giardina, Thierry Mora, Edmondo Silvestri, Massimiliano Viale, and Aleksandra M. Walczak. Statistical mechanics for natural flocks of birds. *Proceedings of the National Academy of Sciences*, 109(13):4786–4791, 2012.

[88] Yael Katz, Kolbjorn Tunstro, Christos C. Ioannou, Cristian Huepe, and Iain D. Couzin. Inferring the structure and dynamics of interactions in schooling fish. *Proceedings of the National Academy of Sciences*, 108(46):18720–18725, 2011.

[89] Jacques Gautrais, Christian Jost, and Guy Theraulaz. Key behavioural factors in a self-organised fish school model. In *Annales Zoologici Fennici*, volume 45, pages 415–428. BioOne, 2008.

[90] Charlotte K. Hemelrijk and Hanno Hildenbrandt. Schools of fish and flocks of birds: their shape and internal structure by self-organization. *Interface focus*, 2(6):726–737, 2012.

[91] C. Buhl, D. J. T. Sumpter, I. D. Couzin, J. J. Hale, E. Despland, E. R. Miller, and S. J. Simpson. From disorder to order in marching locusts. *Science*, 312(5778):1402–1406, 2006.

[92] Christopher W. Weimer, J. O. Miller, and Raymond R. Hill. Agent-based modeling: An introduction and primer. In *2016 Winter Simulation Conference (WSC)*, pages 65–79, Dec 2016.

[93] Jeremy Lemus and Subhradeep Roy. The effect of simultaneous auditory and visual sensing cues in a two-dimensional vicsek model. In *Dynamic Systems and Control Conference*, volume 84287 of *V002T30A005*. American Society of Mechanical Engineers, American Society of Mechanical Engineers, 10 2020.

[94] Bahar Afsharizand, Pooya H. Chaghoei, Amirhossein A. Kordbacheh, Andrey Trufanov, and Golamreza Jafari. Market of stocks during crisis looks like a flock of birds. *Entropy (Basel, Switzerland)*, 22, Sep 2020.

[95] L. H. Miranda-Filho, T. A. Sobral, A. J. F. de Souza, Y. Elskens, and Antonio R. de C. Romaguera. Lyapunov exponent in the vicsek model. *Physical Review E*, 105:014213, Jan 2022.

[96] M. Land. Motion and vision: Why animals move their eyes. *Journal of comparative physiology. A, Sensory, neural, and behavioral physiology*, 185:341–52, 11 1999.

[97] B.H. Lemasson, J.J. Anderson, and R.A. Goodwin. Collective motion in animal groups from a neurobiological perspective: The adaptive benefits of dynamic sensory loads and selective attention. *Journal of Theoretical Biology*, 261(4):501–510, 2009.

[98] Laura Kloepper, Yang Liu, and John R. Buck. Bottlenose dolphins direct sonar clicks off-axis of targets to maximize fisher information about target bearing. *The Journal of the Acoustical Society of America*, 138(3 Supplement):1843–1843, 09 2015.

[99] Fei Liu, Zihao Lu, and Xianke Lin. Vision-based environmental perception for autonomous driving. *ArXiv*, abs/2212.11453, 2022.

[100] Assia Benbihi, Matthieu Geist, and Cedric Pradalier. Learning sensor placement from demonstration for uav networks. *2019 IEEE Symposium on Computers and Communications (ISCC)*, pages 1–6, 2019.

[101] Sayantan Pramanik, Vishnu Vaidya, Gajendra Malviya, Sudhir Sinha, Shripad Salsingikar, M Girish Chandra, C V Sridhar, Godfrey Mathais, and Vidyut Navelkar. Optimization of sensor-placement on vehicles using quantum-classical hybrid methods. In *2022 IEEE International Conference on Quantum Computing and Engineering (QCE)*, pages 820–823, Sep. 2022.

[102] Eric Bonabeau, Marco Dorigo, and Guy Theraulaz. *Swarm Intelligence: From Natural to Artificial Systems*. Oxford University Press, 10 1999.

[103] Gerardo Beni and Jing Wang. Swarm intelligence in cellular robotic systems. In Paolo Dario, Giulio Sandini, and Patrick Aebischer, editors, *Robots and Biological Systems: Towards a New Bionics?*, pages 703–712, Berlin, Heidelberg, 1993. Springer Berlin Heidelberg.

[104] Timothy Chung and Roshan Daniel. Darpa offset: A vision for advanced swarm systems through agile technology development and experimentation. *Field Robotics*, 3:97–124, 01 2023.

[105] Robert Brown and Julie A. Adams. Congestion analysis for the darpa offset ccast swarm. *Field Robotics, Special Issue: Dynamic Large-Scale Swarm Systems in Urban Environments: Results from the DARPA OFFSET Program*, 2023.

[106] Jacques Gautrais, Francesco Ginelli, Richard Fournier, Stéphane Blanco, Marc Soria, Hugues Chaté, and Guy Theraulaz. Deciphering interactions in moving animal groups. *PLOS Computational Biology*, 8(9):1–11, 09 2012.